Climate Dynamics
https://doi.org/10.1007/s00382-023-06835-2

Impacts of land-surface heterogeneities and Amazonian deforestation on the wet season onset in southern Amazon

Juan Pablo Sierra[1] · Jhan-Carlo Espinoza[1] · Clementine Junquas[1] · Sly Wongchuig[1] · Jan Polcher[2] · Vincent Moron[3,4] · Lluís Fita[5] · Paola A. Arias[6] · Anthony Schrapffer[5] · Romain Pennel[2]

Received: 3 August 2022 / Accepted: 17 May 2023

Abstract
Continued Amazonian deforestation perturbs the surface turbulent fluxes which are important for building the conditions for the wet season onset in the southern Amazon. This work evaluates the impacts of tropical deforestation on the onset and development of the Amazonian rainy season using a weather typing approach. We use 19-year simulations (2001–2019) with the Regional Earth System Model from the Institute Pierre Simone Laplace (RegIPSL) with twin control/deforestation experiments. RegIPSL represents the dominant modes or the atmospheric circulation patterns (CPs) of the daily-to-decadal circulation variability in tropical South America, and the evolution of atmospheric and surface conditions along the dry-to-wet transition period. According to RegIPSL, forests and crops contribute differently to the onset. During the dry-to-wet transition period, croplands/grasslands present a stronger shallow convection driven by a higher atmospheric temperature. Large-scale subsidence suppresses low-level convection in the region and deep convection only persists over forests where the atmosphere presents more convective potential energy. After the onset and the establishment of large-scale rainfall structures, both land covers behave similarly in terms of surface fluxes. Deforestation decreases the frequency of the CP typically linked to the onset. Changes in the spatial structure and frequency of the wet season CPs reinforce the hypothesis of a deforestation-induced dry season lengthening. Variations in the CP frequency and characteristic rainfall have opposite effects on accumulated rainfall during the dry-to-wet transition period. Whereas alterations in frequency are associated with a regional circulation response, changes in the CP characteristic rainfall correspond to a local response to deforestation.

Keywords Amazon deforestation · Wet season onset · Climate modeling · Land-surface heterogeneities · Atmospheric circulation

1 Introduction

The Amazon rainforest is an important driver in the climate system. Exchanges of water and energy within and through the borders of the largest tropical rainforest in the world help to sustain the atmospheric circulation in the tropics and precipitation in the South American continent (Gill 1980; Eltahir and Bras 1994; Eltahir 1996; Gedney and Valdes 2000; Bonan 2008; Fisher et al. 2011; Zemp et al. 2014). The constant anthropogenic pressures such as deforestation,

✉ Juan Pablo Sierra
juan-pablo.sierra-perez@univ-grenoble-alpes.fr;
juanpablosierrap@gmail.com

[1] Université Grenoble Alpes, IRD, CNRS, Grenoble INP, Institut Des Géosciences de L'Environnement (IGE, UMR 5001), Grenoble, France

[2] LMD/IPSL, École Polytechnique, Institut Polytechnique de Paris, ENS, PSL Research University, Sorbonne Université, CNRS, Palaiseau, France

[3] Aix-Marseille University, CNRS, IRD, INRAE, Collège de France CEREGE, Aix-en-Provence, France

[4] Lamont-Doherty Earth Observatory, International Research Institute for Climate and Society, Columbia University, Palisades, NY, USA

[5] Centro de Investigaciones del Mar y la Atmósfera (CIMA), UBA-CONICET IRL IFAECI/CNRS-IRD-UBA-CONICET, Buenos Aires, Argentina

[6] Grupo de Ingeniería Y Gestión Ambiental (GIGA), Escuela Ambiental, Facultad de Ingeniería, Universidad de Antioquia, Medellín, Colombia

Published online: 26 May 2023

global warming and the increase in the extreme weather and climate events during the last decades threaten this mega biodiverse ecosystem and raise the concern on the possible impacts of the Amazonian degradation on the regional and global climate (Malhi and Wright 2004; Cox et al. 2008; Malhi et al. 2008; Brienen et al. 2015; Shukla et al. 2019; Arias et al. 2021).

During the last six decades, population growth, agriculture and cattle ranching expansion, logging, mining, as well as road and dam building have led to continuous deforestation in the Amazon region (Fearnside 1993; Hutyra et al. 2005; Nepstad et al. 2008; Latrubesse et al. 2017). By the year 2011, around 87% of the Amazon basin was still covered by original forest (Davidson et al. 2012) while it has been reduced to 83% in 2020 (Eiras-Barca et al. 2020; Souza et al. 2020). Major clearance areas are located in the southern and eastern parts of the basin conforming the so called 'arc of deforestation' (Malhi et al. 2008; Leite et al. 2011; Davidson et al. 2012). The southern Amazon, which encompasses between 30 and 40% of the basin, has experienced one of the most rapid agricultural expansion in the world (Salazar et al. 2007; Instituto Nacional De Pesquisas Espaciais 2014). Taking into account that observations and models estimate that between 24 and 41% of the Amazonian precipitation originates from local evapotranspiration (Salati et al. 1979; Eltahir and Bras 1994; Dirmeyer and Brubaker 2007; Van Der Ent et al. 2010; Staal et al. 2018; Dominguez et al. 2022), deforestation could have profound implications in the regional hydrology.

The southern Amazonia, defined here as the region between 5°S–15°S and 70°W–50°W (Fig. 1a, b), is characterized by a strong rainfall annual cycle and a weak evapotranspiration seasonality (Fig. 2a, b, respectively), both driven by the seasonal warming and the establishment of regional-scale features such as the South American Monsoon System (SAMS) (Horel et al. 1989; Figueroa and Nobre 1990; Liebmann and Marengo 2001; Espinoza et al. 2009). The dry season in the region occurs between June–August, when rainfall rate is around 1 mm day^{-1} (Fig. 2a). As a consequence of water and energy limitations, evapotranspiration is minimum during these months (Fig. 2b; Juárez et al. 2007). A rapid precipitation increase from August to October characterizes the dry-to-wet transition period (Marengo et al. 2001). At the same time, evapotranspiration rises following the increments in precipitation, incoming solar radiation and net surface radiation (Fig. 2c and i; Myneni et al. 2007), what contributes to preconditioning the atmosphere for the arrival of the wet season (Li and Fu 2004; Yin et al. 2014; Wright et al. 2017). Many authors suggest that the evapotranspiration increase during this period moistens the boundary layer and increases the available potential energy of the lower troposphere (Fu et al. 1999; Li and Fu 2004; Li et al. 2006). Cold fronts entering to Amazonia from the extratropics lift warm and humid surface air over

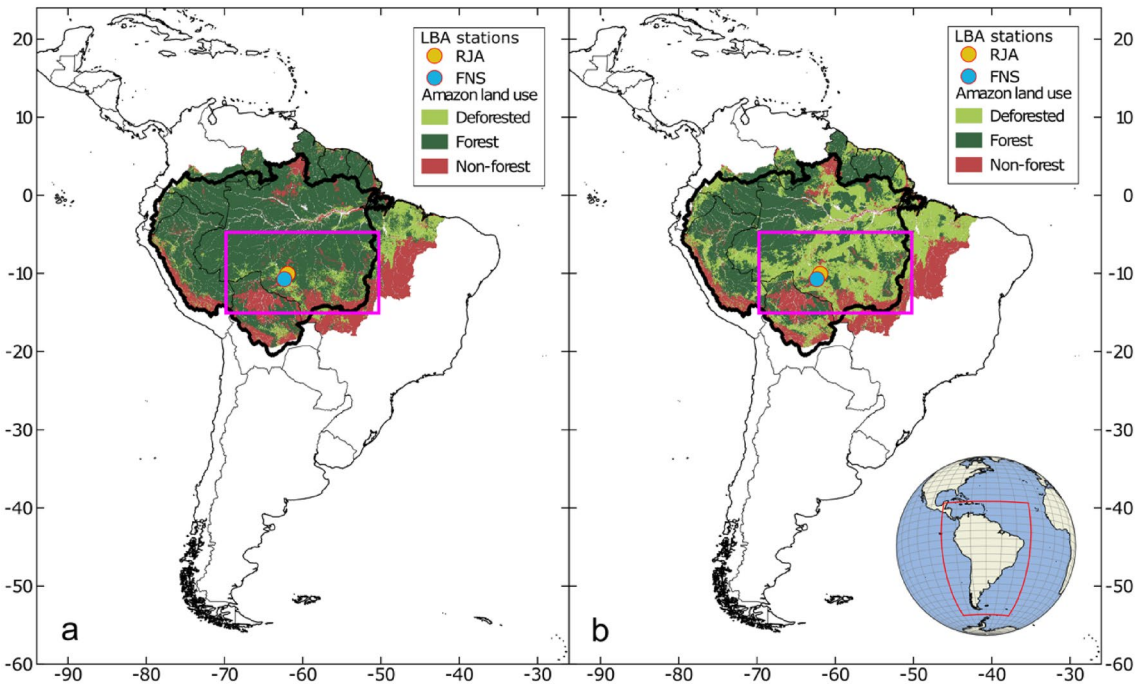

Fig. 1 Experiment scenarios: **a** Control and **b** Deforested. RegIPSL simulation domain is shown in the left bottom corner in panel **b**. Magenta box shows the southern Amazon region (5°S–15°S, 70°W–50°W) defined to compute the annual cycle in Fig. 2. Blue and yellow circles in **a** and **b** show the location of the flux towers from the Large-Scale Biosphere–Atmosphere experiment in the Amazon

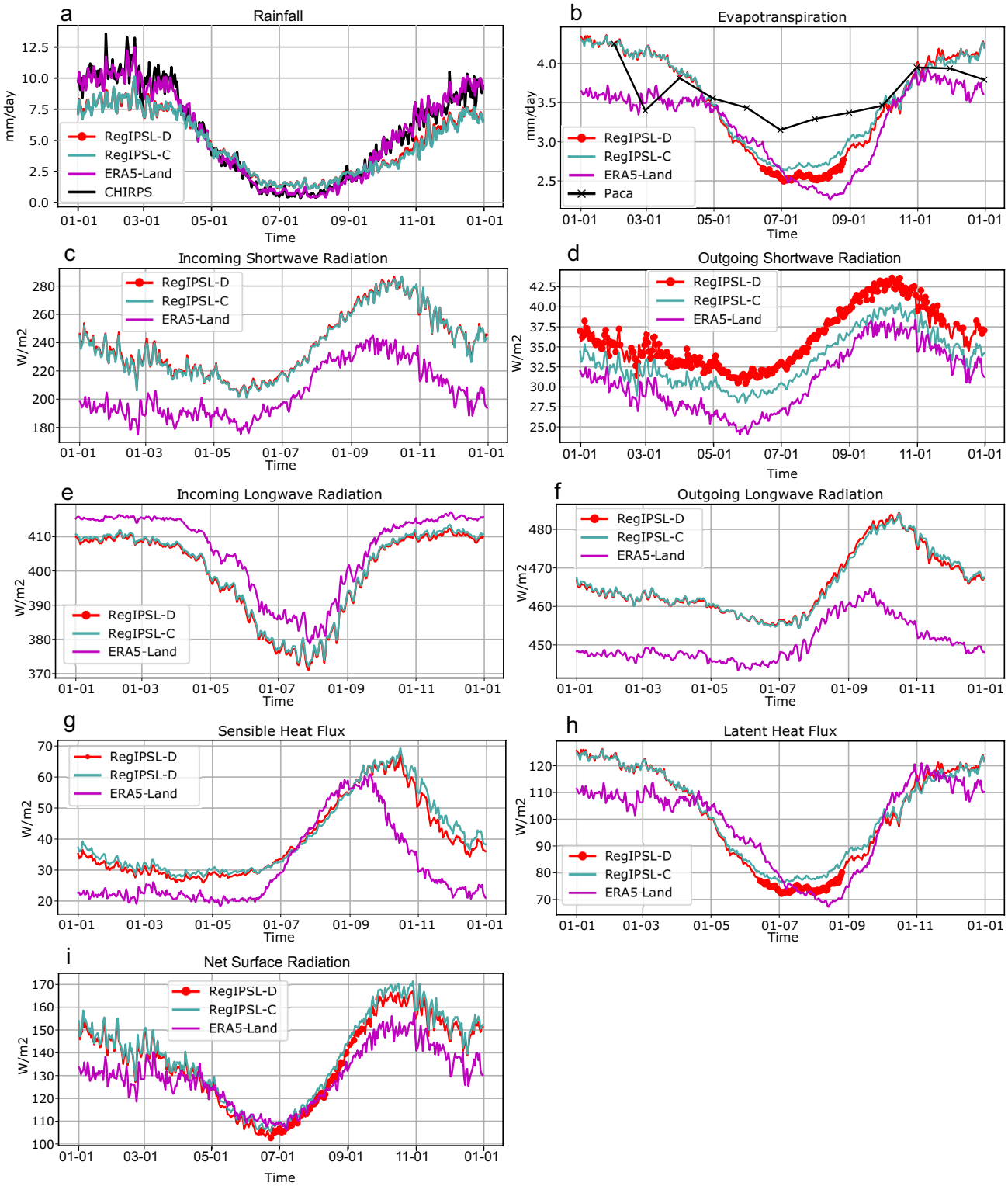

Fig. 2 Annual cycle in southern Amazon (see Fig. 1) for: **a** rainfall and **b** evapotranspiration in mm day^{-1}, **c** incoming shortwave radiation, **d** outgoing shortwave radiation, **e** incoming longwave radiation, **f** outgoing longwave radiation, **g** sensible heat flux and **h** latent heat flux, and **i** net surface radiation (in W m^{-2}). Cyan and red lines represent RegIPSL-Control and RegIPSL-Deforested, respectively. Significant changes (t-test, $p < 0.05$) between RegIPSL-Control and RegIPSL-Deforested are marked with red dots. Black lines represent reference datasets CHIRPS and Paca in **a**–**b**, and magenta lines represent reanalysis ERA5-Land in **a**–**i**

the southern Amazon, and trigger deep convection setting up the wet season onset (Li and Fu 2006; Espinoza et al. 2013). Rainy events associated with cold intrusions during the early wet season warm the atmosphere through diabatic heating driving the reversal of the cross-equatorial flow and enhancing advection of moisture laden winds from the Atlantic Ocean in a positive feedback (Wang and Fu 2002). As a result, the core of the wet season is observed during December-February, when precipitation reaches more than 8 mm day^{-1} (Fig. 2a; Marengo et al. 2001; Gan et al. 2004; Yin et al. 2014).

Drier conditions have been reported over the southern Amazon in the recent decades in terms of: (1) an increase in dry days frequency during the dry-to-wet transition period (Espinoza et al. 2019; Funatsu et al. 2021); (2) an increase in tree's mortality and biomass degradation (Brienen et al. 2015); and (3) shorter wet and larger dry seasons since the 1970's (Phillips et al. 2009; Fu et al. 2013; Debortoli et al. 2015; Arias et al. 2015; Correa et al. 2021). This lengthening of the dry season is related to multiple causes that include alterations in the entrance of cold fronts to the Amazon basin and the latitudinal location of the Southern Hemisphere subtropical jet (Fu et al. 2013), the Atlantic and Pacific sea surface temperatures and its inter-annual/decadal variability (Arias et al. 2015; Marengo et al. 2017), atmospheric circulation changes in the Hadley and Walker cells (Yoon and Zeng 2010; Barichivich et al. 2018; Agudelo et al. 2019; Espinoza et al. 2021) and the human-induced influence of the forest-to-cropland conversion (Butt et al. 2011; Debortoli et al. 2015; Ruiz-Vásquez et al. 2020). Natural forests over the region are vulnerable to a lengthening of the dry season and to reductions in total annual rainfall (Da Silveira Lobo Sternberg 2001; Sombroek 2001; Staver et al. 2011; Guan et al. 2015). Indeed, year-to-year variations in the onset of the wet season affect river flows, fire risk, small-scale agriculture, methane emissions due to alterations of the flood pulse and the inter-annual variability of the global atmospheric CO_2 concentrations (Cochrane et al. 1999; Asner 2009; Lee et al. 2011; Chen et al. 2011; Molina-Carpio et al. 2017; Melack et al. 2022). Although in agreement with observations, coupled biosphere–atmosphere models suggest a delay in the date of the wet season onset under deforestation scenarios (Costa and Pires 2010; Boisier et al. 2015; Nobre et al. 2016; Alves et al. 2017; Ruiz-Vásquez et al. 2020; Commar et al. 2023), these works are limited by the fact that they are based on the analysis of modeled parameterized rainfall with coarse horizontal resolutions.

Among all the perturbations induced to surface energy and water fluxes by forest loss, deforestation decreases the net radiative energy at the surface, and consequently the evapotranspiration and latent heat flux according to flux-tower and satellite-derived data (von Randow et al. 2004, 2020; Khand et al. 2017; Baker and Spracklen 2019; Oliveira et al. 2019; Laipelt et al. 2020). A reduction in the vegetation's transpiration (the water loss through the plant's leaves) is caused also by the reduced soil–water-uptake capacity of the shorter crop roots (Neill et al. 2013; Caioni et al. 2020). On the other hand, deforestation favors the occurrence of shallow clouds and reduces deep convection activity during the dry and dry-to-wet transition season (Wang et al. 2009). Both evapotranspiration and deep convection during these particular months are important for the onset and evolution of the rainy season. Thus, in this study we analyze how deforestation can perturb the onset and development of the wet season in southern Amazonia.

A recent study has explored the observed dry season lengthening over the southern Amazon under a pattern recognition framework of weather typing or atmospheric circulation patterns (CPs) approach (Espinoza et al. 2021). The CPs can be understood as regional-scale circulation anomalies which are recurrent and correspond to preferred states of the climate system (Moron et al. 2008, 2015; Espinoza et al. 2021). Espinoza et al. (2021) explained the lengthening of the dry season in the southern Amazonia in terms of an increased frequency of a particular CP linked to enhanced subsidence over southern tropical South America and a decreased occurrence of a CP characterized by the entry of cold intrusions and convective activity over the region (Fig. 2 in Espinoza et al. 2021). Taking into account that wind circulation is usually better represented by climate models in comparison with precipitation (Kendon et al. 2012; Flato et al. 2013; Fosser et al. 2015; Pichelli et al. 2021; Ban et al. 2021), using the circulation pattern approach results attractive to explore deforestation experiments with a regional climate model. Therefore, this study evaluates the impacts of Amazonian deforestation on the onset and evolution of the rainy season in the southern Amazon, based on CPs, using a control and a deforested experiment with the Regional Earth System Model of the Institute Pierre Simon Laplace (RegIPSL). This work is organized as follows: the control and deforestation experiments, as well as the data and methods are described in Sect. 2; Sect. 3 is dedicated to validating the model in terms of (1) the annual cycle of rainfall and surface fluxes in the southern Amazon, (2) the regional atmospheric circulation variability through the CPs, and (3) the conditions in the atmospheric circulation states, rainfall and evapotranspiration during the onset of the wet season; we end the section with a discussion of the role of the land-surface heterogeneities on the development of the wet season onset; in Sect. 4, we assess the impacts of deforestation on the evolution of the Amazonian wet season; finally, Sect. 5 discuses and summarizes the main results.

2 Data and methods

2.1 Model description

RegIPSL (https://gitlab.in2p3.fr/ipsl/lmd/intro/regipsl/regipsl/-/wikis/home) is an Earth system model that couples the atmospheric model Weather Research and Forecasting Model (WRF), the land surface model ORganising Carbon and Hydrology In Dynamic EcosystEms (ORCHIDEE), and the oceanic model Nucleus for European Modelling of the Ocean (NEMO). The coupling between the different modules of the model is performed by OASIS-MCT (Craig et al. 2017) and input/output is done via the XML-IO-SERVER (XIOS, https://forge.ipsl.jussieu.fr/ioserver). However, the present work does not use the oceanic component.

The atmospheric regional climate model WRF version 3.7.1 is used in this study (Skamarock et al. 2008). The WRF model can be implemented for both research and forecast activities. WRF is extensively used to dynamic downscaling purposes in South America (e.g. Spera et al. 2018; Trachte 2018; Posada-Marín et al. 2019; Saavedra et al. 2020; Junquas et al. 2022; Rosales et al. 2022; Dominguez et al. 2022) and to analyze deforestation impacts on the regional climate (e.g. Bagley et al. 2014; Eghdami and Barros 2019; Eiras-Barca et al. 2020; Sierra et al. 2021). This is a non-hydrostatic model with terrain-following vertical coordinates. In our configuration, the model presents 50 vertical levels (model top at 10 hPa), a 60 s running time step and a horizontal resolution of 20 km × 20 km encompassing the South American continent (Fig. 1a, b). Table 1 summarizes the general configuration of the model.

After different preliminary sensitivity tests (not shown), the physical parameterizations chosen in this work include the RRTMG radiation scheme (Iacono et al. 2008), the Morrison 2-moment scheme for cloud microphysics and dynamics of water species (Morrison et al. 2009), the Mellor Yamada MYNN level 2 scheme for the planetary boundary and surface layers (Nakanishi and Niino 2006) and the convection scheme Grell Freitas (Grell and Freitas 2014). To simulate the effects of land cover change on the interactions between soil/vegetation and the atmosphere, WRF is coupled with the land surface model ORCHIDEE (Krinner et al. 2005; Maignan et al. 2011). ORCHIDEE resolves the processes of the energy and water balances at the surface, as well as the evolution of the vegetation and the carbon cycle. In this sense, it represents the vegetation mechanisms that control the carbon assimilation and determine vegetation state and its evaporative capacity. Table 2 summarizes the complete WRF's set-up.

Boundary conditions are extracted from the fifth generation reanalysis of the European Centre for Medium-Range Weather Forecast (ECMWF) ERA5 (Hersbach et al. 2020). With a higher spatial and temporal resolution (31 km × 31 km horizontal grid size, 137 hybrid sigma-pressure levels and data each hour, respectively), ERA5 improves the representation of several atmospheric processes, including the vertical structure of winds and humidity, and more consistent soil moisture, evaporation and sea surface temperatures with respect to its predecessor ERA-Interim (Hoffmann et al. 2019; Hersbach et al. 2020). This data set is available at https://www.ecmwf.int/en/forecasts/datasets/reanalysis-datasets/era5 (last access July 2022). In order to constrain the large-scale meteorological conditions in WRF simulations toward the synoptic circulation at the domain boundaries, we use spectral nudging (von Storch et al. 2000) above the planetary boundary (at scales above 1200 km) over horizontal winds and temperature (Miguez-Macho et al. 2004; Zhang et al. 2022). Omrani et al. (2015) recognize that the horizontal wind is the most important

Table 1 Characteristics of the WRF simulations

Model version	3.7.1
Horizontal resolution (km)	20
Number of vertical levels	50
Run time step (s)	60
Output time resolution (h)	3
Domain center coordinates	21° 6′ 36″ S 60° 17′ 60″ W

Table 2 Physical configuration of the WRF simulations

	Parameterizations	References
Radiation	Longwave-shortwave RRTMG radiation scheme	Iacono et al. (2008)
Cumulus	Grell Freitas scheme	Grell and Freitas (2014)
Planetary boundary layer	Mellor Yamada MYNN 2	Nakanishi and Niino (2006)
Cloud microphysics	Morrison 2-moment scheme	Morrison et al. (2009)
Surface layer	MYNN Scheme	Nakanishi and Niino (2006)
Land surface	ORCHIDEE	Krinner et al. (2005)

variable to nudge in order to improve the representation of surface temperature, wind and precipitation.

In the present study, each component of the RegIPSL coupled model and the coupled model itself are initiated in a different way. For the atmospheric component we perform a 1-year simulation with WRF. The outputs of this simulation are used as a forcing for the spin-up of the off-line land surface model ORCHIDEE. Due to the slow evolution of soil dynamics and the strong impact of land surface conditions on the performance of regional climate models, several studies suggest the use of an off-line spin-up for the land surface model (Smith et al. 1994; Cosgrove et al. 2003; de Goncalves et al. 2006; Sutton et al. 2006; Case et al. 2008). We implement an off-line 10-year spin-up for ORCHIDEE based on the outputs from the 1-year WRF run. Finally, we use the restarts from the 1-year WRF and 10-year ORCHIDEE simulations as initial conditions for the regional coupled climate model for both control and deforestation experiments. The first coupled year of each experiment is not used and is considered as the spin-up of the coupled model.

2.2 Description of the experiments

In order to obtain a representative view of the long-term atmospheric intra-seasonal variability, we use 19 years of simulations covering the period 2001–2019. For this period, we perform two simulations sharing the same boundary forcing from ERA5 but with different land-use conditions. The control experiment (hereafter 'RegIPSL-Control' or 'RegIPSL-C') utilizes information of the annual evolution of land-use/cover from the European Space Agency Climate Change Initiative (ESA-CCI) land-cover maps (ESA 2017; Lamarche et al. 2017). This data set, originally covering the period 1992–2015, was recently extended until 2020 by the Copernicus Climate Change Service. It presents a 300 m × 300 m spatial resolution. The 22 land-cover ESA-CCI classes were reclassified into 13 Plant Functional Types (PFTs) required by the ORCHIDEE model (Bontemps et al. 2013).

On the other hand, the deforested experiment (hereafter 'RegIPSL-Deforested' or 'RegIPSL-D') is based on future projections of Amazonian deforestation developed by Soares-Filho et al. (2006). In the present study, the Business-As-Usual (BAU) scenario for the year 2050 was used (Fig. 1b). This scenario is the result of an empirically-based modeling study where 1997–2002 deforestation rates derived from satellite imagery were projected (Soares-Filho et al. 2006). Additional assumptions include paving all planned highways, the lack of new protected areas in the basin, and empirical relationships involving the forest loss probability and the proximity to roads, rivers and towns, as well as already deforested patches. This deforestation scenario is widely used for the assessment of the influence of land use changes on the hydrology and climate of the South American continent (Coe et al. 2009; Swann et al. 2015; Eiras-Barca et al. 2020; Sierra et al. 2021). Despite the existence of new Amazon deforestation scenarios, the high spatial resolution, the deep knowledge of the socio-political dynamics at the regional level on which it is based, and the geographic extension covered make Soares-Filho BAU scenario still suitable as a pessimistic deforestation projection. Among the new databases on Amazon deforestation projections are the deforestation scenarios from the CMIP5 project. For its most pessimistic scenario (RCP8.5), deforestation in the Amazon has been found to be too low, reaching only 20% total deforestation by 2050 (Pires et al. 2016). Using satellite data, Souza et al. (2020) have reported deforestation estimations close to this value for 2017 over the Brazilian Amazon. Another recent study has developed a series of updated deforestation scenarios based on local information on recent political and socio-economical dynamics (Rochedo et al. 2018). However, their deforestation projections have the limitation of being defined only for the Brazilian Amazon and not for the entire Amazon basin as in the case of Soares-Filho.

The BAU data set from Soares-Filho has a 1 km × 1 km horizontal resolution and labels each pixel as forest, deforested or non-forest. Since the ORCHIDEE PFTs maps have a coarser resolution (20 km × 20 km), all BAU scenario pixels within each PFTs grid cell were used to calculate the forest/deforested ratio. Then, to each PFT pixel in the control experiment, we impose this calculated ratio to the existent proportion between the classes 'tropical broad-leaved evergreen' and 'C3 agriculture'. Our premise is that deforestation is a change from forest to agricultural crops. In this sense, we keep unaltered the areas of the rest of land cover classes and only modify the area covered by forest and crops. Modifications to the PFTs were made for each year in both control and deforested experiments.

2.3 Reference datasets

In order to assess the model performance, we use rainfall, evapotranspiration and surface energy variables such as incoming/outgoing shortwave and longwave radiation, sensible/latent heat fluxes and surface net radiation obtained from ERA5-Land (Muñoz-Sabater et al. 2021). This data set is the product of numerical integrations of the ECMWF land surface model forced with the downscaled atmospheric forcing from ERA5 reanalysis. ERA5-Land has an enhanced horizontal resolution of ~ 9 km × 9 km at hourly scales, with data available from 1950 to present. ERA5-Land presents improvements in latent heat fluxes, Bowen ratio, skin temperature and soil moisture with respect to ERA5 (Muñoz-Sabater et al. 2021). To compare the model surface fluxes against *in-situ* measurements at a local scale,

we use flux tower measurements from the Large-Scale Biosphere–Atmosphere Experiment in the Amazon (LBA) project (Saleska et al. 2013). The LBA project was an international project initiated in 1998 as a scientific effort to better understand, among other questions, the effects of land use changes in the Amazon on the regional climate. Two stations located inside our region of interest, the southern Amazon (5°S–15°S, 70°W–50°W, magenta box in Fig. 1a, b), were selected from the LBA data base. Located at 10.75° S, 62.35° W, and 306 m a.s.l., the station *Fazenda Nossa Senhora de Aparecida* (blue circle labeled as 'FNS' in Fig. 1a, b), corresponds to a cattle ranch over a deforested area. Additionally, the station *Rondonia Jaru Biological Reserve* is located at 191 m a.s.l., 10.08° S, 61.93° W (yellow circle labeled as 'RJA' in Fig. 1a, b). This station is located inside a natural reserve created by the Brazilian government in the 1960's. These stations present daily record of surface energy and water fluxes for the period 1999–2002. However, only the years 2001 and 2002 that overlap in time with our simulations are used. This dataset is available at https://daac.ornl.gov/LBA/guides/CD32_Brazil_Flux_Network.html (last access July 2022).

We use rainfall information from the Climate Hazards Group InfraRed Precipitation with Station data (CHIRPS) data set version 2 (Funk et al. 2015). Developed by the United States Geological Survey (USGS) and the Earth Resources Observation and Science (EROS), this data set is the result of a combination between satellite measurements, rain gauges data and interpolation techniques. Its high spatial and temporal resolutions (5 km × 5 km and daily data, respectively), as well as its long record period from 1981 to 2020, makes this data set suitable to analyze the precipitation-atmospheric flow regime relationship at high temporal frequencies. When compared against rain gauges and in situ discharge measurements, CHIRPS exhibits a good representation of Amazon hydrology (Wongchuig Correa et al. 2017; Haghtalab et al. 2020). Therefore, this database is widely used to study the rainfall variability over tropical South America (e.g. Paccini et al. 2018; Cerón et al. 2020; Arias et al. 2020; Funatsu et al. 2021). The dataset is available at https://data.chc.ucsb.edu/products/CHIRPS-2.0/ (last access July 2022).

In order to evaluate the actual evapotranspiration in the southern Amazon, we use the data base developed by Paca et al. (2019), hereafter called 'Paca'. By merging several global remote sensing evapotranspiration products, this data set presents a high resolution (250 m × 250 m) description of the spatial variability within the Amazon basin. Monthly values are provided for the 2003–2013 period and are available at www.wateraccounting.org (last access July 2022). Validated against flux tower measurements from the LBA project, this dataset captures the observed spatial and temporal evapotranspiration variability at monthly and inter-annual scales (Paca et al. 2019). Since there are significant discrepancies among evapotranspiration datasets that reflect the uncertainties in evapotranspiration estimations (Maeda et al. 2017; Sörensson and Ruscica 2018; Fassoni-Andrade et al. 2021), the use of a data based on different products is a way of dealing with the inter-product uncertainty. A more complete validation of the representation of evapotranspiration annual mean and annual cycle by RegIPSL model can be found in Wongchuig et al. (2023; submitted to Journal of Hydrology).

2.4 Definition of the large-scale circulation patterns (CPs)

The definition of the CPs is based on unfiltered daily meridional and zonal wind components at 850 hPa over the region 10°N–30°S, 90°W–30°W. Adding other variables in the CP's definition (such as temperature, rainfall or geopotential height) increases the computation cost and does not improve the classification of the atmospheric states related to precipitation (Espinoza et al. 2012). Horizontal winds at 850 hPa have proven to be suitable for the description of the main atmospheric circulation phenomena in tropical South America, such as the easterly winds, the southern regimes or 'cold surges', the South American Low-level Jet (SALLJ), among others (Paccini et al. 2018). In addition, winds at 850 hPa (around 1500 m of altitude) are most of the time located within the Planetary Boundary Layer (PBL) and, therefore, should not be affected by the imposed large-scale nudging in our model experiments. As a first step, horizontal winds are standardized using the long-term mean and standard deviation at each grid-cell so keeping all the time variations including the seasonal cycle. In order to accelerate computations and to retain only the main variability modes, we apply principal component analysis over standardized winds from ERA5, RegIPSL-Control and RegIPSL-Deforested independently. The principal component approach has been used in previous studies to filter out the smallest spatial scales of the regional-scale atmosphere's phase space (Moron et al. 2008, 2015; Olmo et al. 2022). We use the 30 leading principal components, which explain 78% and 73% of the total variability for ERA5 and RegIPSL-Control/Deforested, respectively, to identify the CPs using the *k*-means methodology.

K-means is a dynamical clustering procedure that looks for classifying data into *k* clusters in an n-dimensional subspace, in this case, spanned by the 30 leading principal components. The *k* clusters are selected by recursive iterations that seek to minimize the sum of variance between points belonging to the same cluster (Diday and Simon 1976). Defining the number of groups or clusters to be used is a key question in clustering analysis. Different indices have been designed in order to find the optimal number of clusters, all of them sharing the basic principle:

identifying the number of clusters with greatest similarity between the members of a cluster and with the highest inter-cluster difference (Calinski and Harabasz 1974; Michelangeli et al. 1995). Previous studies have demonstrated that a number of 9 CPs are appropriated to represent the main stages of the annual regional-scale circulation in northern South America (da Anunciação et al. 2014; Paccini et al. 2018; Espinoza et al. 2021). Following Espinoza et al. (2021), we define 9 clusters to summarize the regional atmospheric variability, considering all times scales from daily to decadal. In this sense, the 6935 days of our interest period 2001–2019 are classified in 9 groups or CPs. The assignment of each day to a particular CP is, up to a certain point, dependent to the *k*-means methodology, specifically to initial cluster centroids used for starting the classification or 'initialization' (Michelangeli et al. 1995). For this reason, 1000 reclassifications of the 6935-day time series were performed independently for ERA5, RegIPSL-Control and RegIPSL-Deforested using random initial seeds on each day-classification. For most of the analysis in the present work, we use a particular classification using a smart way to select the initial cluster centers in order to speed up the convergence (Pedregosa et al. 2011). However, for the assessment of changes in the CPs annual cycle frequency in Sect. 4, we use the 1000 classifications in order to evaluate whether the signal induced by deforestation is consistent and independent of the statistical classification method. Finally, composite analysis of interest variables (such as rainfall or evapotranspiration) is carried out over the days belonging to each CP.

2.5 Definition of the wet season onset in the southern Amazon

The onset of the wet season is estimated based on the methodology developed in Li and Fu (2004). We first compute the spatial mean of daily rainfall over the southern Amazon. Then, pentad rainfall time series are estimated by temporally averaging over 5-day period in order to reduce the synoptic noise. According to Li and Fu (2004), the dry season end/wet season onset is established when 6 out of 8 preceding pentads are below the climatological rain rate annual mean and 6 out of 8 subsequent pentads are above it. However, in most of the years there are few consecutive pentads that meet these two conditions. Li and Fu (2004) define the wet season onset as the earliest date or the first of these pentads. Nevertheless, in order to assure that wet conditions begin to be dominant and well established, instead of using the earliest pentad we use the date of the latest pentad fulfilling these conditions as the date of the onset. This analysis is performed independently for CHIRPS and RegIPSL (using data during the same periods).

2.6 Evaluation framework

The assessment of the model's skill in representing the observed CPs, taking as a reference ERA5 for winds, and CHIRPS for precipitation, is performed through the analysis of the spatial patterns of CP composite means, as well as their climatological frequency of occurrence along the year.

The evaluation of the CP spatial pattern is addressed by comparing the mean composite fields from reference datasets and RegIPSL Control using Taylor diagrams. Taylor diagram is a graphical tool that summarizes the match between two spatial or temporal fields in terms of the Pearson correlation, the root-mean-square error and the ratio of their variances (Taylor 2001). This methodology is widely used in climate modeling studies (e.g. Voldoire et al. 2013; Sierra et al. 2015; Ortega et al. 2021; Olmo et al. 2022). For each CP we compare separately the spatial distribution of rainfall, zonal and meridional winds.

On the other hand, following Olmo et al. (2022), the representation of the CP frequencies of occurrence is analyzed with an error metric that quantifies the absolute difference between the climatological daily frequencies in the reanalysis and model outputs (Eq. 1). This metric is computed for each CP and can be estimated as:

$$Error_{CP} = \frac{\sum_{i=1}^{D} \left| fERA5_{CP_i} - fRegIPSL_{CP_i} \right|}{D} \quad (1)$$

where D is the total number of days during the evaluated season. A special attention is paid to the dry-to-wet transition (July–November). In this period D corresponds to 153 days. Then, i is an index for dates varying between July 1st and November 31st. $fERA5_{CP_i}$ and $fRegIPSL_{CP_i}$ are the number of days corresponding to a specific CP for the date i in the whole 2001–2019 period for ERA5 and RegIPSL respectively. For example, for i corresponding to July 1st, and analyzing the representation of the CP T1, $fERA5_{CP_i}$ represents the number of times that T1 is observed on this particular date in the whole 19-year period. A similar interpretation applies for $fRegIPSL_{CP_i}$.

3 Model validation

In this section, we show the validation of the RegIPSL-Control simulations in terms of the annual cycle of rainfall and surface fluxes in the southern Amazon. The dominant modes of the regional low-level circulation variability in tropical South America and the model's skill to reproduce the meteorological conditions for the onset of the wet season are also assessed. For this purpose, we use *in-situ* LBA measurements, satellite and reanalysis data.

3.1 Rainfall and surface fluxes in the southern Amazon

The seasonality of precipitation over the southern Amazon is well represented by RegIPSL-Control, with rainfall maxima during December–February according to observations as described in Sect. 1 (cyan line in Fig. 2a). During this season, the model underestimates the rainfall rates by about − 20% (− 2.4 mm day^{-1}) with respect to CHIRPS and ERA5-Land. On the contrary, precipitation minimum is simulated and observed in June–August, with an overestimation of about + 120% (+ 0.46 mm day^{-1}) in this particular season. As a consequence, the steep rainfall switch in both dry-to-wet and wet-to-dry transition periods is weaker in RegIPSL-Control than in CHIRPS and ERA5-Land. For example, during the dry-to-wet transition between September 1st and November 1st, mean rainfall increases at a rate of 2.50 mm day^{-1} per month in CHIRPS, and only about half of this value (1.21 mm day^{-1} per month) in the model. Nevertheless, since our study focuses on atmospheric circulation patterns for characterizing the wet season onset instead on rainfall, particular emphasis will be placed on biases on wind circulation of the model (Sect. 3.2).

The mean evapotranspiration annual cycle is well represented by RegIPSL-Control compared with Paca and ERA5-Land estimates, with maximum and minimum fluxes during the wet and dry seasons respectively (cyan line in Fig. 2b). RegIPSL does not capture the bimodal regime observed in Paca et al. (2019), although it represents a small peak in October when maximum incoming solar and net surface radiation are simulated (Fig. 2c and i). Additionally, the general amplitude of the seasonal cycle is higher in RegIPSL-Control, ranging between 2.67 and 4.27 mm day^{-1}, compared to Paca et al. (2019), with values between 3.15 and 4.25 mm day^{-1}. Similar to RegIPSL-Control, evapotranspiration in ERA5-Land varies between 2.34 and 3.85 mm day^{-1}. Differences among evapotranspiration data sets have been reported by previous works and reflect the uncertainty, the lack of data and the need of a better-understanding of the vegetation evaporative capacity in the Amazon basin and in the tropics in general (Maeda et al. 2017; Sörensson and Ruscica 2018; Fassoni-Andrade et al. 2021). A more complete assessment of the representation of evapotranspiration by RegIPSL can be found in Wongchuig et al. (2023; submitted to Journal of Hydrology).

On the other hand, RegIPSL-Control shows a realistic representation of the seasonal cycle of incoming and reflected solar radiation fluxes (cyan line in Fig. 2c–d). The incoming solar radiation is overestimated in about + 30 W m^{-2} or + 12% along the year. This error is probably caused by an underestimation of the cloud cover. Less clouds in the model outputs are also linked with a drier atmosphere which radiates less energy to the ground, causing an underestimation of the incoming longwave radiation (Fig. 2e). A little lag in the peak of the incoming solar radiation is part of the model outputs. While maximum incoming solar radiation occurs in the middle of September in ERA5-Land, it is located in October in RegIPSL-Control. Since this is energy flux is the only energy input to the surface that exhibits a delay, we hypothesize that this bias is related to the slightly lagged peak in outgoing longwave radiation and sensible heat (Fig. 2f–g). The possible mechanism behind this bias could be related again to problems in the representation of clouds. Cloudiness could be larger in RegIPSL in September than in October, in contrast to ERA5, what can cause an underestimation (overestimation) of the incoming solar radiation during September (October). On the other hand, although more energy reaches the ground in terms of solar radiation, the underestimation of the incoming longwave radiation and the overestimation of the outgoing longwave flux help to balance the energy budget and, at the end, the net surface radiation is well represented in seasonality and magnitude. However, an overestimation by RegIPSL-Control is observed during the dry-to-wet and wet seasons in the net surface radiation (Fig. 2i). The overestimation of surface energy fluxes, especially net surface radiation and sensible heat flux seems to be a systematic error in WRF over the Amazon basin regardless of the model configuration (Wang et al. 2021).

Although our main interest is the southern Amazonia as a whole region, the model validation up to now is strongly based on a model to model comparison. For this reason, we also analyze the representation of surface fluxes at a more local scale using the selected flux towers from the LBA project, located over one forested and one deforested site (Fig. 1a, b). The distance between the two LBA stations is 87 km. Thereby, we use a surrounding area of 100 km × 100 km (5 × 5 grid cells) encompassing the measurements sites for surface fluxes from RegIPSL-Control outputs. Then, we select grids with forest or cropland fractional areas higher than 70%, in order to compare the model against the forested and deforested LBA sites for the years 2001–2002. The results of this analysis are shown in Figure S1 and reflect the same model biases observed at a regional scale described previously (except for rainfall). At local scale, RegIPSL-Control and observations present the same rainfall seasonality, with a wet season in December-May and a dry season in June–August. However, the model exhibits a strong rainfall overestimation during the wet season over forested and deforested areas (Fig. S1a, b). Similar to the behavior exposed by Paca et al. (2019) at a more regional scale, evapotranspiration shows little seasonality with fluctuations around the 2.5 mm day^{-1} and 3 mm day^{-1} over the forest and pasture LBA sites, respectively (Fig. S1c, d). Higher precipitation rates in RegIPSL-Control causes an evapotranspiration overestimation between January and

May. Evapotranspiration overestimation is higher over croplands in the model outputs. Nevertheless, the model is able to represent the weak seasonality of this surface water flux along the year. Most of the surface energy variables are realistically represented in terms of magnitude and seasonality (Fig. S1e–n). However, RegIPSL-Control overestimates the incoming solar radiation between August to November, with a slightly higher bias over the forest site (Fig. S1f). As a consequence, the model also overestimates the outgoing or reflected solar radiation over the forest site (Fig. S1h). In addition, the model slightly underestimates (overestimates) the incoming (outgoing) longwave radiation flux along the year over both areas in a similar way to the regional analysis shown previously (Fig. S1i–l). Nevertheless, in the same way that at regional scale, these errors compensate each other, and the net surface radiation is well represented by the model (Fig. S1m, n).

3.2 Main circulation patterns (CPs) in tropical South America

In this sub-section, we show if the model is able to capture the dominant modes of the regional circulation variability over tropical South America. The regional atmospheric circulation variability is summarized through 9 CPs that can be understood as preferred states of the regional climatic system (Figs. 3 and 4). As described by Espinoza et al. (2021), there is a clear seasonal cycle in the relative CPs frequency (Fig. 3). We identify 3 CPs with major activity during austral summer, corresponding to the wet season in the southern Amazon, labeled as W1–W2–W3 (blue colors), 3 austral winter CPs with usual dry conditions and largest frequencies in June–August, labeled D1–D2–D3 (orange–red colors), and 3 transitional CPs characterizing mostly the dry-to-wet transition $T2_{DW}$ (dark green), the wet-to-dry shift $T3_{WD}$ (yellow) and a CP that occurs in both transitional periods T1 (green color). Table 3 summarizes the main features of the circulation and rainfall anomalies associated with each atmospheric state or CP. A more exhaustive description of the CPs low-level circulation and atmospheric mechanisms is presented by Espinoza et al. (2021).

As seen in Fig. 3b, RegIPSL-Control is able to properly represent the relative CP's frequency along the year even if the classification is done independently from ERA5. Differences in the CP's frequency during the dry-to-wet transition period (July–November) between ERA5 and RegIPSL-Control are quite small and do not surpass ± 1 day of mean error (Table S1). It is interesting to note that higher frequency errors are presented during the transition CPs T1 and $T2_{DW}$. Similar results were reported recently by Olmo et al. (2022) for the representation of the same transitional CPs by last generation global climate models.

Figure 4 shows low-level horizontal wind and rainfall anomalies (vs the annual mean) for each CP according to RegIPSL-Control. A direct comparison with ERA5/CHIRPS composites (Fig. S2), as well as the Taylor diagrams analysis (Fig. S3), allows us to conclude that RegIPSL-Control captures well the spatial structure of wind and rainfall patterns associated with all CPs. Indeed, spatial correlations for the CP composites with respect to reference datasets are significantly high (> 0.78) as seen in the Taylor diagrams in Fig. S3. Precipitation is the variable with the lowest spatial correlations, mainly during the transition CPs T1 and $T2_{DW}$ (0.79 and 0.81, respectively; Fig. S3a). The spatial distribution of horizontal winds at 850 hPa is well represented by the model for all circulation patterns (spatial correlation > 0.95; Fig. S3b, c), except for the meridional component of D2. This particular CP presents a strong meridional component of

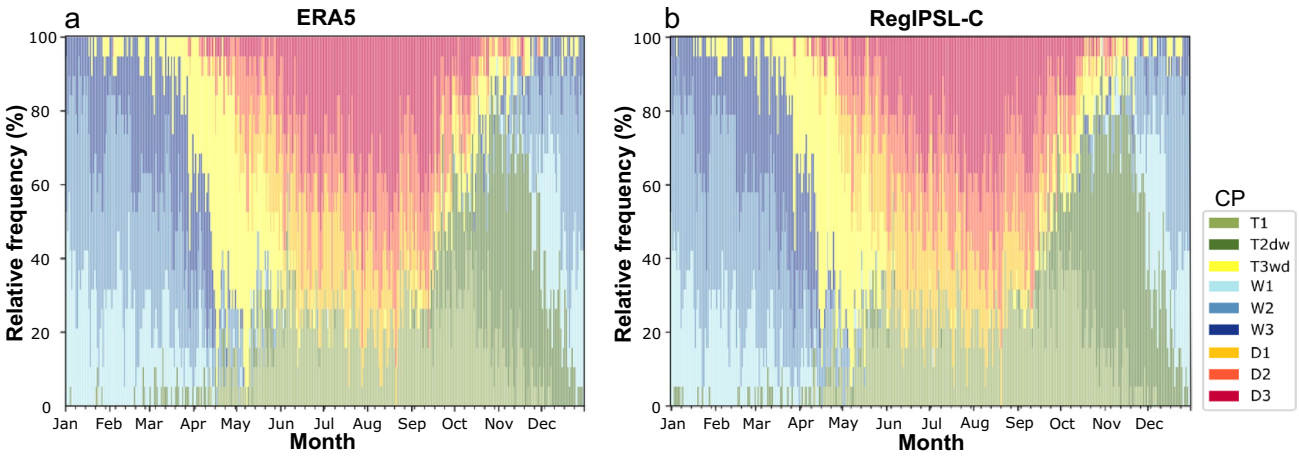

Fig. 3 Relative mean daily frequency of the 9 circulation patterns (CPs) defined from the k-means clustering analysis for: **a** ERA5, and **b** RegIPSL-Control (RegIPSL-C). The horizontal axis represents the days from January 1st to December 31st in the climatology during the period 2001–2019

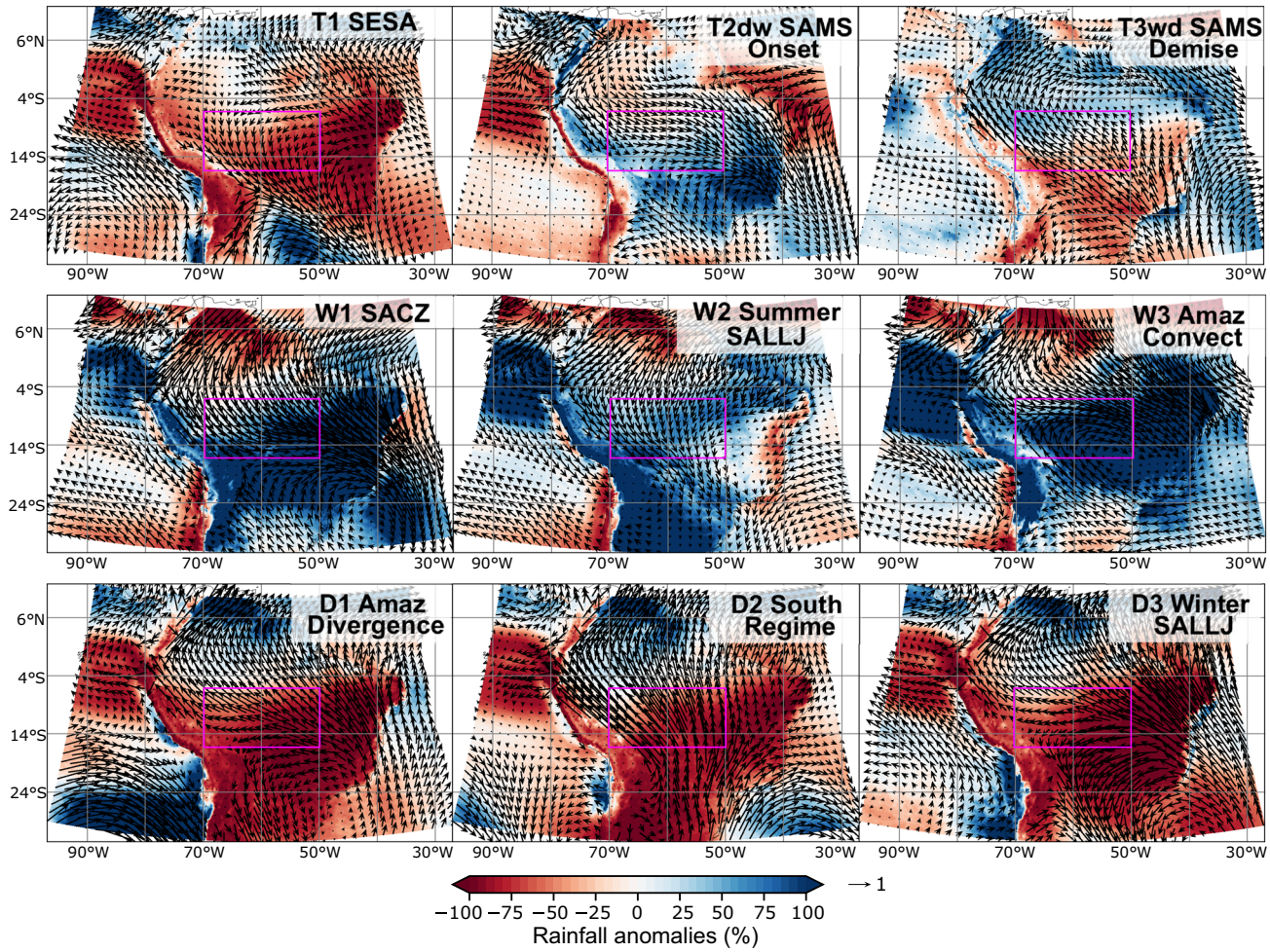

Fig. 4 Rainfall and 850 hPa horizontal wind anomalies (vs the annual mean) composites for the 9 circulation patterns (CPs) defined from the k-means clustering analysis using RegIPSL-Control outputs. Rainfall (shaded) is in percentage respect to the inter-annual mean and horizontal winds at 850 hPa (vectors) are adimensional. Magenta box shows the southern Amazon (5°S–15°S, 70°W–50°W)

the wind that characterizes the entry of the so called 'cold fronts' into tropical South America coming from the southern part of the continent (see Table 3). For this reason, this CP is more sensitive to the representation of the meridional wind. In order to better explore the biases in RegIPSL outputs, we compute the differences in low-level winds and rainfall with respect to ERA5 and CHIRPS as seen in Fig. 5.

In general, rainfall composite differences between RegIPSL-Control and CHIRPS are rather constant across the transitional and wet season CPs (Fig. 5). The model exhibits lower precipitation rates over Colombia and Ecuador while overestimates it in northeastern Amazonia and northern Brazil (Fig. 5). Rainfall is also underestimated by RegIPSL-Control over the South Eastern South America region (SESA, defined as the continental area east of the Andes below 23°S) during T1, W2 and D3 events. These circulation patterns are very related with the activity of the SALLJ (see Table 3) which suggests a bad representation of the link between rainfall and the SALLJ circulation in La Plata basin. Recent works demonstrate that adding the representation of floodplains to the RegIPSL model can result in a better representation of precipitation and the moisture transport by the SALLJ in La Plata basin (Schrapffer 2022). In the same way, precipitation biases are similar among the wet season CPs. While less rainfall is simulated over the central Amazon and the Guianas, higher rainfall is simulated over the eastern Brazil.

Wind differences between RegIPSL-Control and ERA5 in tropical South America are higher for the dry and transition season CPs (Fig. 5). For CPs T1, $T3_{WD}$ and D2, the spatial distribution of wind differences between RegIPSL-Control and ERA5 are very similar to their mean patterns shown in Fig. 4. This implies that the model presents a stronger regional circulation and overestimates the 850 hPa winds over the entire region on these particular meteorological conditions. $T3_{WD}$ and $T2_{DW}$ present no statistically

Table 3 Brief overview of the main features of the CPs explaining the atmospheric circulation variability in tropical South America identified by Espinoza et al. (2021). D1, D2, D3 (W1, W2, W3) correspond to dry (wet) season CPs

Seasonality	Intra-seasonal variability			
	Dry season or austral winter CPs	D1	D2	D3
		-Major frequency during the early dry season (June) -Positive (negative) rainfall anomalies over northern (southern) tropical South America -Low-level wind divergence centered in the southwestern Amazon and related to southerly cross-equatorial wind	-Major frequency during the core of the dry season (July–August) -Positive (negative) rainfall anomalies over northern (southern) tropical South America and the northwestern Amazon -Anomalous southerly cross-equatorial regime coming from the subtropics linked to cold intrusions	-Major frequency during the late dry season (August) -Positive (negative) rainfall anomalies over northern (southern) tropical South America -Low-level wind divergence centered in the southwestern Amazon and related to southerly cross-equatorial wind. Development of a winter SALLJ
	Wet season or austral summer CPs	W1	W2	W3
		-Major frequency during the early wet season (December) -Positive rainfall anomalies over the continental South Atlantic Convergence Zone (SACZ) and most of the tropical Andes -Anomalous northerly cross-equatorial flow deviated eastward due to the encounter with southerly wind intrusion	-Major frequency during the core of the wet season (December-February) -Positive rainfall anomalies in South Eastern South America (SESA), the Amazon-Andes rainfall hotspots and the Andes -Anomalous northerly cross-equatorial winds reaching southern latitudes of tropical South America related to the summer SALLJ	-Major frequency during the late wet season (February–March) -Positive rainfall anomalies over the Amazon basin and the tropical Andes -Anomalous northerly cross-equatorial flow encountering southerly wind intrusion and generating convergence over the Amazon basin
	Transitional CPs	T1	T2DW	T3WD
		-Major frequency during the wet-to-dry (May–June) and dry-to-wet (September–October) periods -Positive rainfall anomalies over South Eastern South America (SESA) and negative anomalies over the southern Amazon and eastern Brazil -Intensified South American Low-level Jet (SALLJ) below 14°S	-Major frequency in the dry-to-wet transition (October–November) -Positive rainfall anomalies over the southern Amazon and southeastern Brazil -Anomalous northerly cross-equatorial winds encountering a southerly wind incursion	-Major frequency in the wet-to-dry transition (April–May) -Positive (negative) rainfall anomalies over the northern (southern) south America -Anomalous southerly cross-equatorial winds from tropical south Atlantic

Transitional CPs are labeled T1, $T2_{DW}$ (transition from dry-to-wet conditions) and $T2_{WD}$ (transition from wet-to-dry conditions). See Figure S2 in supplementary material for rainfall and wind composites with ERA5/CHIRPS

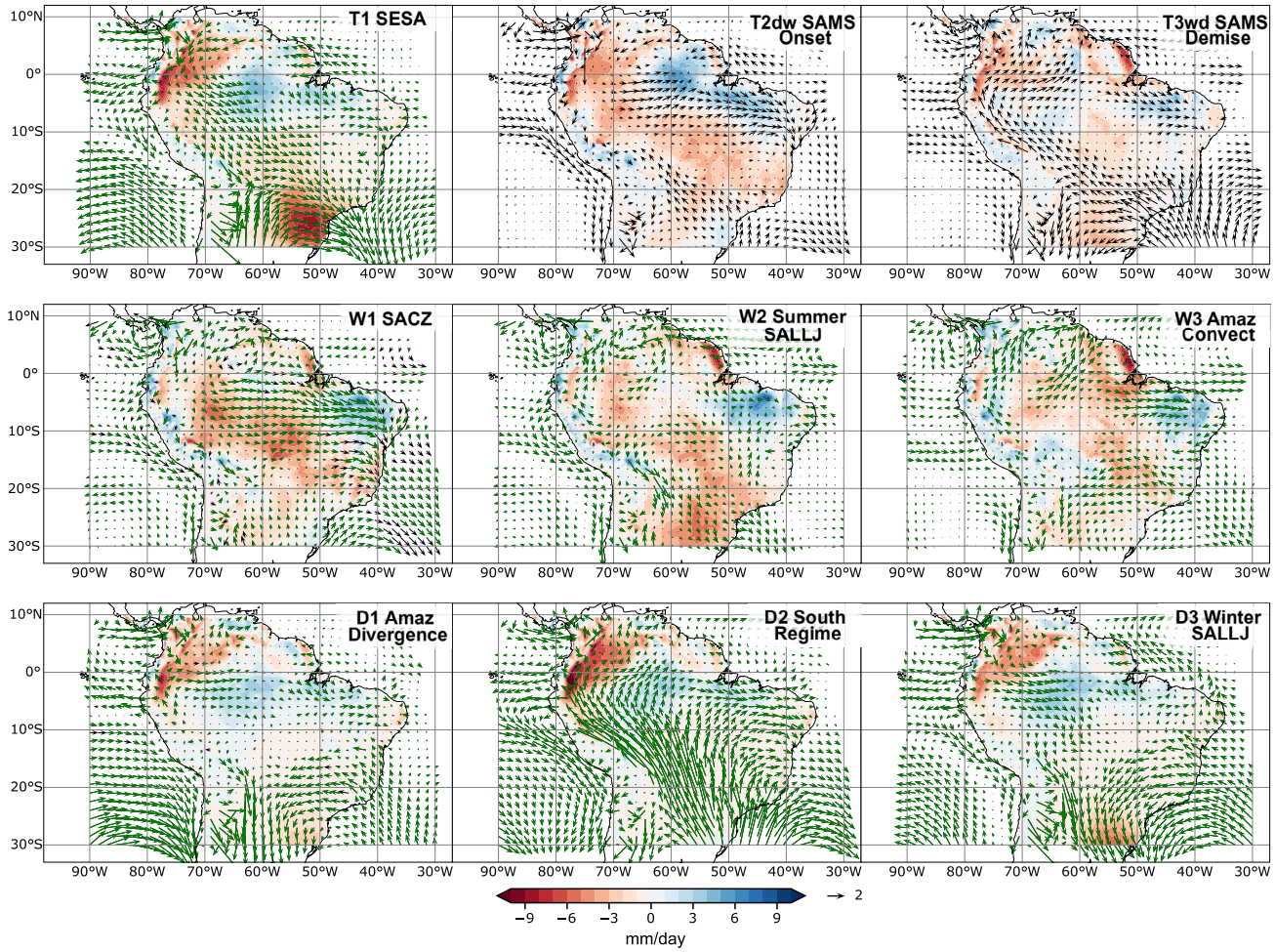

Fig. 5 Rainfall and 850 hPa horizontal wind anomalies composites differences RegISPL-Control minus ERA5/CHIRPS for the 9 circulation patterns (CPs) defined from the k-means clustering analysis. Rainfall differences (shaded) are in mm day^{-1} and horizontal winds at 850 hPa (vectors) are in m s^{-1}. Only significant rainfall differences are shown (t-test, $p < 0.05$). Green vectors represent significant wind differences (t-test, $p < 0.05$)

significant wind differences with respect to ERA5 despite their relatively high wind differences (Fig. 5) which suggests a large low-level wind variability during these particular transitional atmospheric patterns. A stronger low-level circulation during the dry and dry-to-wet transition seasons in RegIPSL could be related to a high model sensitivity to the external synoptic signal from ERA5 boundary forcing. Indeed, D1 and D3 display stronger southward winds blowing from southwestern Amazon toward the La Plata basin in RegIPSL-Control. Contrary to winter CPs, summer CPs (W1–W2–W3) present little wind differences with respect to ERA5.

3.3 Wet season onset characteristics in terms of CPs

This subsection analyzes the conditions in the atmospheric circulation states, rainfall and evapotranspiration during the preceding and subsequent days of the wet season onset in reanalysis dataset and RegIPSL-Control.

Figure 6a shows the evolution of CP frequency throughout the development of the wet season onset (defined in Sect. 2.5). Around 90 days before the onset, nearly 80% of the days are under winter or dry conditions (D1, D2 and D3), according to ERA5. Precipitation in southern Amazonia (see Fig. 1a, b for the location) is almost zero before the day − 90 (i.e. 90 days before the wet season onset), whereas evapotranspiration is near its minimum (Fig. 6c, d). After the day − 80, dry season CPs start to be less frequent and are replaced by $T3_{WD}$ and mainly by $T2_{DW}$ (Fig. 6a). In this sense, by the day − 75, dry season CPs occur 80% of the time while transitional regimes $T3_{WD}$ and $T2_{DW}$ are not observed. Nonetheless, after 25 days (by the day − 50), dry season and transitional CPs occur 61% and 12% of the time, respectively. At the same time, rainfall and evapotranspiration begin to increase (Fig. 6c, d). Consistent with our

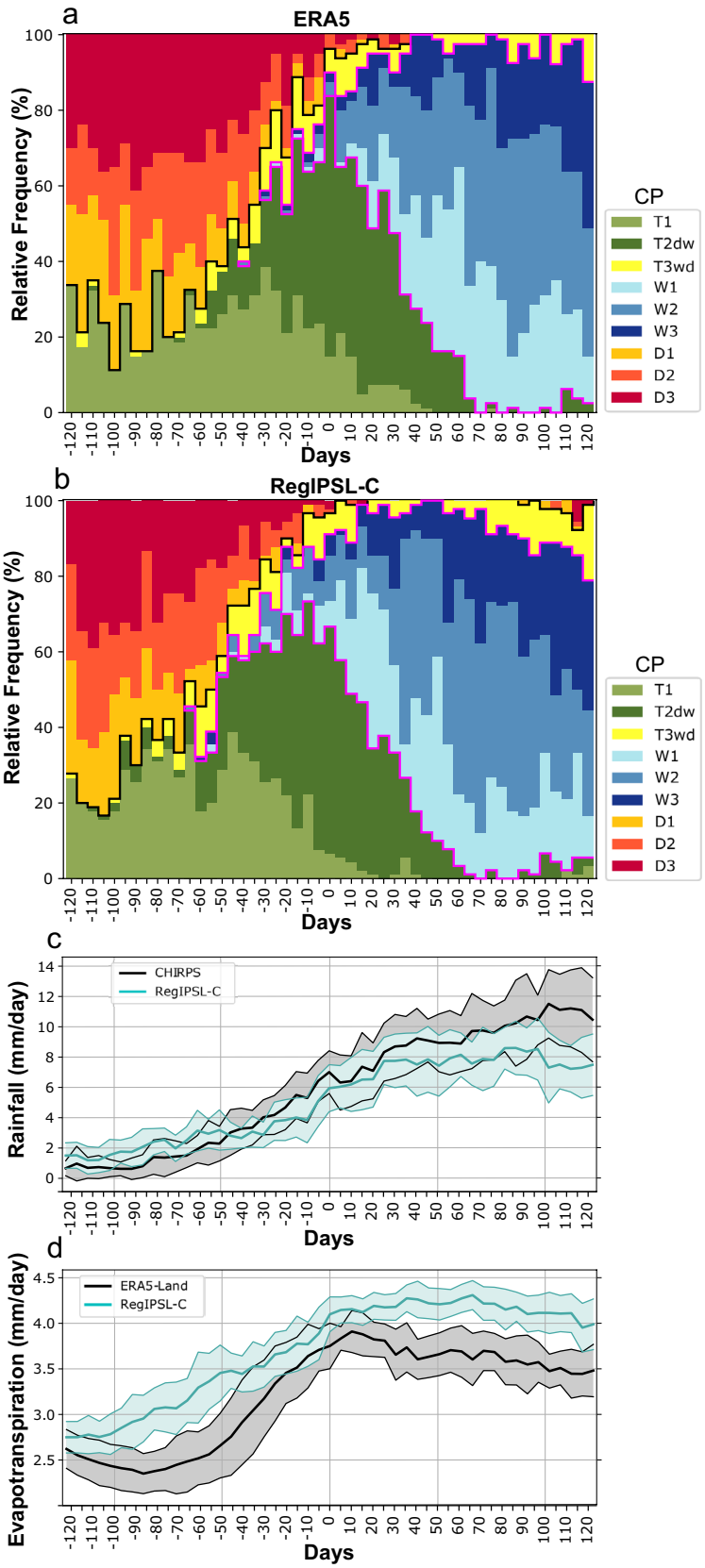

Fig. 6 Composite time series of: **a** and **b** relative frequency of circulation patterns from **a** ERA5 **b** RegIPSL-Control, taking as a reference the date of the wet season onset in southern Amazonia (day 0); **c** rainfall and **d** evapotranspiration for reference datasets in black solid lines (CHIRPS for rainfall, and ERA5-Land for evapotranspiration) and RegIPSL-Control (cyan solid lines) in mm day^{-1}. The x-axis represents the time, with negative (positive) values for days before (after) the onset. Gray and cyan envelopes represent the standard deviation at inter-annual scale for reference datasets and RegIPSL, respectively. Black and magenta lines in **a** and **b** enclose the dry and wet season CPs respectively

results, previous works locate the end of the dry and the beginning of the dry-to-wet transition season about 90 days before the onset, when the atmosphere starts to moisten and the lower troposphere begins to gain (reduce) available potential energy (the convective inhibition) (Fu et al. 1999; Li and Fu 2004; Wright et al. 2017). The incoming solar radiation increases rapidly until the day − 60, and then a slower increment is sustained until its maximum in the day − 25 for ERA5-Land (not shown). It is precisely after the day − 25 when the steep evapotranspiration increment flattens out slightly in ERA5-Land (Fig. 6d). Thus, because of the combination of positive incoming solar radiation anomalies over the southern Amazon (related to a higher frequency of T1, $T2_{DW}$ and D3; not shown) and positive precipitation anomalies (linked to the presence of $T2_{DW}$ during this period; see Fig. 4) there is a rapid evapotranspiration increase between days − 60 and − 25. The role of the solar radiation on the rainforest's response in terms of evapotranspiration during the transition from dry to wet season is reported in observational-based works (Myneni et al. 2007). On the other hand, precipitation presents a stronger increase between the days − 60 and 0, when $T2_{DW}$ starts to be more frequent during this period. Wright et al. (2017) find a rainfall and evapotranspiration increase between 60 to 30 days before the onset in consistency with our results. A peak in the frequency of $T2_{DW}$ (64%) is observed precisely at the onset of the wet season (pentad 0; Fig. 6a). Previous studies demonstrate the relationship between the variability of the Amazonian wet season onset and the frequency of $T2_{DW}$ (Espinoza et al. 2021). In fact, our $T2_{DW}$ looks very similar to circulation anomalies registered by early works during the wet season onset in the southeastern Amazon, with enhanced trade winds in the Atlantic, southern wind intrusion in the Amazon and more rainfall in central and southern parts of the basin (see Figs. 10, 11 of Marengo et al. 2001). According to Wright et al. (2017), the last 30 days before the onset mark a shift from shallow to deep convection. During this period, CP W1, W2 and W3 begin to appear and develop deep convection in the region (Fig. 6a). Five days after the SAMS onset, summer or wet season CPs are observed during ~ 20% of the time and by the day + 50, they occur 80% of the time (about 60% is occupied by the presence of the SACZ-SALLJ dipole corresponding to the W1-W2 co-existence).

The model shows a realistic development of the different characteristics of the wet season onset (Fig. 6b–d). However, there are some differences in the simulated development of the wet season in RegIPSL-Control. The model exhibits an early retreat of the dry or winter circulation patterns around the day − 105, and consequently, an early development of the transitional CP $T2_{DW}$. While in ERA5, around the day − 95, dry season CPs (D1–D2–D3) account for 80% of total frequency, in the model these atmospheric wintertime regimes account for only 62%. Likewise, at this time, the transitional CP $T2_{DW}$ is absent in the reanalysis but in the model, it is observed prematurely 8% of the time. Similarly, the evapotranspiration and rainfall start to increase around 20 days in RegIPSL-Control before the reference data sets (Fig. 6c, d). Consistently, wet season circulation patterns W1–W2–W3 start to appear also 20 days early in the model simulation. However, similarly to ERA5, the model exhibits the major activity of CP $T2_{DW}$ around the onset date (day 0), with a 62% of frequency.

One limitation of the previous rainfall and evapotranspiration analysis is the homogenization of meteorological variables through spatially averaging over a big area. The southern Amazon is characterized by the juxtaposition of rainforest trees and croplands/grasslands. These land surface heterogeneities are determinant for triggering mesoscale circulations and for defining the nature of convective activity, cloudiness and atmospheric stability in this particular region (Cutrim et al. 1995; Silva Dias and Regnie 1996; Souza et al. 2000; Wang et al. 2009). The land cover effect is particularly important during the dry and dry-to-wet transition seasons, when the extratropical cold surges are less frequent and the atmosphere is more stable (Siqueira and Toledo Machado 2004; Wang et al. 2009). Therefore, understanding the evolution of surface fluxes and atmospheric variables over the different land covers is crucial for disentangling their differentiated contribution on the beginning of the wet season onset.

3.4 Wet season onset characteristics over forest and croplands/grasslands

After a validation of the representation of atmospheric circulation states, rainfall and evapotranspiration along the development of the wet season by RegIPSL-Control (see Sect. 3.3), in this section we evaluate the evolution of surface and atmospheric characteristics over different land covers in the region. To this end, we identify and select the areas within the southern Amazonia (see Fig. 1a for location) where forest or croplands/grasslands are the dominant vegetation type. Pixels labeled as 'forest' present a fractional area higher than 60% covered by the 'Tropical Broadleaf Evergreen' category. Similarly, pixels labeled as 'cropland/grassland' correspond to a 60% or more of fractional area covered by the categories 'Temperate Natural Grassland', 'Natural Grassland' and 'C3–C4 Crops'. We compute spatial averages for meteorological variables over forest and cropland/grassland areas separately, as well as composites for the preceding and subsequent days of the rainy season onset (Figs. 7 and S4).

Although the general temporal evolution for most of the variables is similar between forest and crop/grass, there are significant differences in magnitude mainly before the onset of the rainy season. Since forest covers around 92% of the

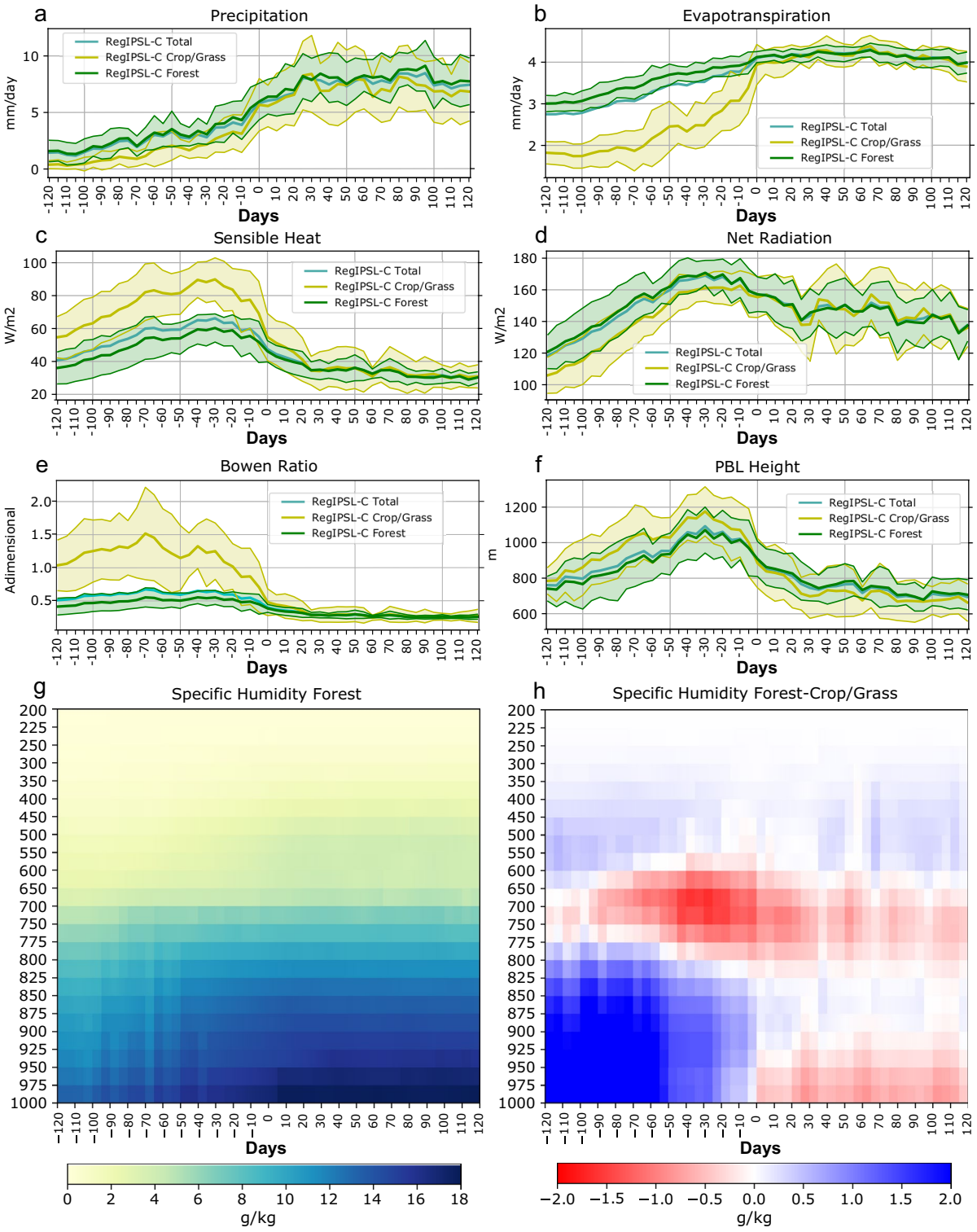

Fig. 7 Composite time series of: **a** precipitation (mm day^{-1}), **b** evapotranspiration (mm day^{-1}), **c** sensible heat flux (W m^{-2}), **d** net radiation (W m^{-2}), **e** Bowen ratio (adimensional), **f** Planetary Boundary Layer (PBL) height (m) over the total southern Amazon, forest and cropland areas (cyan, green and yellow lines, respectively) from RegIPSL-Control. Green and yellow envelopes represent the standard deviation or inter-annual variability for each land cover. Vertical cross-sections of: **g** specific humidity (g kg^{-1}) over forest areas and **h** forest minus crop/grass specific humidity difference (g kg^{-1}), **i** vertical wind component over forest areas (m s^{-1}) and **j** forest minus crop/grass vertical wind component difference (m s^{-1}). The x-axis represents the time, with negative (positive) values for days before (after) the onset

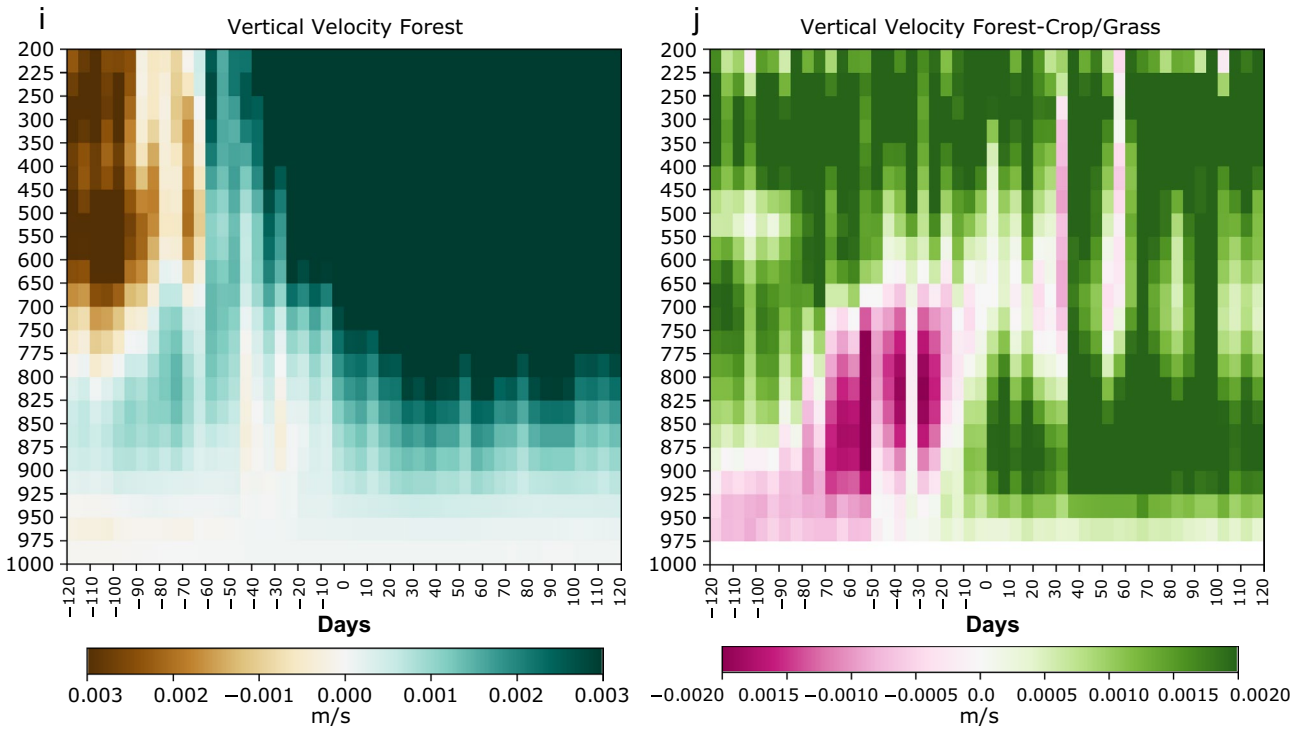

Fig. 7 (continued)

southern Amazon total area, the magnitude and temporal pattern between averages over the forest area and over the total area (green and blue lines in Fig. 7, respectively) are very similar for all the analyzed variables. Reduced precipitation is observed over croplands/grasslands during the whole period but only significant before the day − 25 (Fig. 7a), when wet season CPs W1–W2 start to occur in the model outputs (Fig. 6b). In agreement with *in-situ* observations, evapotranspiration in the control experiment over forest areas is higher than croplands/grasslands during the dry season due to the greater access of forest roots to deep soil water (Wright et al. 1992; Sommer et al. 2002; von Randow et al. 2004). After the arrival of the first rainy events before the onset (between days − 80 to − 50), cropland/grassland evapotranspiration increases rapidly after the atmospheric water input (Fig. 7b). This fast evapotranspiration response after rainy events has been described previously in *in-situ* measurements from the African Monsoon Multidisciplinary Analysis (Lohou et al. 2014). According to these authors, evapotranspiration speed response is dependent on the soil water content during the previous days in an inverse relation, where for drier soils there is a faster response (Lohou et al. 2014). However, after the beginning of the rainy season (day 0) and with the occurrence of wet season CPs, which present positive rainfall anomalies broadly in the region, we observe no difference in the evapotranspiration flux between forest and crop/grass (Fig. 7b). Little difference between evapotranspiration rates over forested and non-forested areas was observed in the Brazilian state of Rondonia during the wet season using MODIS16 in agreement with our results (da Silva et al. 2019).

Sensible heat increases from days − 120 to − 30, reaching its maximum 30 days before the onset and decreasing later in both forest and croplands/grasslands (Fig. 7c). However, croplands/grasslands exhibit significant higher values before the onset in about ~ + 25 W m^{-2}, what has been reported in observations and climate model simulations (Shukla et al. 1990; Polcher and Laval 1994; Gash and Nobre 1997; Fisch et al. 2004; von Randow et al. 2004; Eiras-Barca et al. 2020). Similarly, the net radiation peaks at the day − 30 (Fig. 7d) indistinctly for forests and croplands/grasslands, following the temporal evolution of the incoming solar radiation (Fig. S4a). Nevertheless, crop/grass areas have a reduced net surface radiation (~ − 10 W m^{-2}) in the pre-onset period as a consequence of the enhanced loss of energy from the reflected solar radiation (albedo effect) and the decreased energy entry from the incoming longwave radiation due to a drier atmosphere (Figs. 7d and S4b, c). These deforestation-induced alterations in the surface energy balance have been widely studied and described by previous works (Fig. 7b; Eltahir 1996; Gash and Nobre 1997; Claussen et al. 2001; Berbet and Costa 2003; von Randow et al. 2004). Due to the increased sensible heat flux and the reduced evapotranspiration over crop/grass areas, the Bowen ratio (which

corresponds to the ratio between sensible and latent heat fluxes) is higher than over forest areas before the onset (Fig. 7e). It is interesting to note that the Bowen ratio over forest is always less than 1, which reflects the dominant role of the latent heat flux in the surface energy partition during the entire period. Otherwise, croplands/grasslands present a Bowen ratio higher than 1 until the day − 20, when the increment in rainfall and evapotranspiration reach their maximum rates and when wet season CPs start to be frequent (Figs. 6b and 7a–e). At the rainy season onset, crop/grass and forest present a similar Bowen ratio (Fig. 7e). Although the differences is not significant, the Planetary Boundary Layer (PBL) height is higher over croplands before the onset (Fig. 7f) in response to the increased sensible heat flux and a warming of the low-level troposphere (Fig. S4e–f; Fisch et al. 2004). Consistently with other variables, croplands/grasslands and forest present a similar PBL height after the establishment of the wet season (Fig. 7f).

During the first part of the pre-onset period (days − 120 to − 60), the vertically integrated moisture divergence is similar over croplands/grasslands and forests (not shown). Therefore, the low troposphere (below 800 hPa) is moister over forested areas (Fig. 7g–h) due to the higher forest evapotranspiration rates shown in Fig. 7b. After the day − 50, the combined effect of increased evapotranspiration by croplands/grasslands and the beginning of the regional-scale atmospheric moisture convergence (not shown), which is related to less frequent dry season CPs D1–D2–D3 (Fig. 6b), reduce the gap between forests and pastures in the atmospheric moisture content (Fig. 7h). It is interesting to note the moister air observed over croplands/grasslands at 600–775 hPa for the entire period, with a peak around the day − 30. At the local scale, this forest-crop/grass difference can be explained by the increased moisture removal linked to higher precipitation in forested areas, and by the vertical moisture advection from the surface to the mid-troposphere caused by the intensification of the vertical wind over crops (Fig. 7i, j). However, horizontal moisture advection at these particular levels could also play a role in the forest-crop/grass atmospheric moisture difference.

A shallow ascending motion is simulated over croplands/grasslands by RegIPSL-Control between days − 120 to − 50 (Fig. 7i, j). Weaker vertical upward wind is observed over forested areas but confined in the 900–700 hPa layer. This stronger surface ascending motion over croplands/grasslands seems to be related with the warming of the lower troposphere (Fig. S4e, f), caused by higher sensible heat flux and the lower specific heat capacity of the drier air over these areas. A smaller Convective Inhibition Energy (CINE) over croplands/grasslands during the morning and noon also facilitates the air ascension (not shown). During the same period (days − 120 to − 50), it is also observed a strong subsidence above the 750 hPa linked to the dominant presence of the dry season CPs (Figs. 6b and 7i; Espinoza et al. 2021). This large-scale circulation forcing inhibits the development of convective activity triggered by the local signal. Only until the day − 50, the locally forced ascension can surpass the regional subsidence and generate deep convection, mainly over forest areas (Fig. 7i, j). Although by this time, the vertical component of the wind is higher over croplands below the 700 hPa level, convection is stronger above this level over forested areas as a consequence of a higher Convective Available Potential Energy (CAPE) during the pre-onset period (not shown). Higher CAPE over forested areas is a consequence of a wetter atmosphere, which increases the equivalent potential temperature over the lower atmospheric levels and its vertical gradient (Fig. S4g, h). Higher CAPE and conditional atmospheric instability have been observed over forest sites compared with pasture sites (Taylor and Ellis 2006; Wang et al. 2009). The development of convective systems depends not only on the atmospheric instability, but also on trigger mechanisms allowing the release of the convective available potential energy (Adler et al. 2011). According to our results, we hypothesize that the thermally-induced shallow ascending movement over croplands/grassland can be advected and propagated by the horizontal circulation toward forest neighboring areas, where it acts as a trigger mechanism for developing convection. A similar mechanism is described by Froidevaux et al. (2014) using an idealized cloud-resolving model. When the rainy season onset arrives (day 0), a reduction in the sensible heat flux over croplands/grasslands (Fig. 7c) causes shallower PBL (Fig. 7f), a descending air motion below 850 hPa (Fig. 7j), and an increase in the specific humidity over the shallow troposphere (Fig. 7h).

The land cover-differentiated analysis for the temporal evolution of meteorological variables along the development of the rainy season allow us to identify the following key messages: (1) the temporal variability is similar for croplands/grasslands and forest surfaces for all the analyzed variables and is controlled by regional-scale phenomena; (2) the forest and crop/grass local scale response to the synoptic forcing is different in terms of the magnitude of the variables only before the onset of the rainy season. Therefore, land surface heterogeneities can have a stronger impact on the local circulation during the pre-onset period; (3) with the rainy season onset, the establishment of wet season atmospheric regimes bring rainfall to the whole Amazon basin, which helps to eliminate the local differences associated to land-surface heterogeneities, and generates similar behavior between forests and croplands/grasslands for all the analyzed variables. For this reason, in the following sections we assess the impacts of Amazonian deforestation with an especial focus on the changes of circulation patterns and surface conditions before the onset of the wet season.

4 Deforestation impacts on the dry-to-wet transition season

In this subsection, we analyze the deforestation-induced changes in precipitation, evapotranspiration and low-level wind circulation of the CPs and the consequences of these disturbances on the development and onset of the rainy season. Finally, we determine the individual effect of changes in frequency and characteristic rainfall of the CPs caused by deforestation for the total rainfall accumulated in the 120-day period prior to the onset.

4.1 Rainfall and surface fluxes seasonal cycles over the southern Amazon

The loss of tropical forest causes important changes in evapotranspiration and surface energy fluxes, while only little rainfall alterations are simulated over southern Amazonia (Fig. 2). Although not significant, rainfall slightly increases between October and November in the deforested experiment (red line in Fig. 2a). However, deforestation induces significant reductions in evapotranspiration and latent heat fluxes (red line in Fig. 2d–h) of about ~ − 5 to − 6% during the dry season in consistency with flux tower measurements, satellite and meteorological reanalysis estimates (von Randow et al. 2004, 2020; Khand et al. 2017; Baker and Spracklen 2019; Oliveira et al. 2019; Laipelt et al. 2020) and climate models (Nobre et al. 1991; Polcher and Laval 1994; Sud et al. 1996; Lean and Rowntree 1997; Perugini et al. 2017; Eiras-Barca et al. 2020). It is important to remark that differences between RegIPSL-Control and the reference datasets (ERA5-Land and Paca data base) are higher than those between control and deforested experiments what reflects the current challenges in evapotranspiration estimations. The sensible heat flux is slightly increased in the deforested scenario in the dry-to-wet transition in agreement with observations (Fig. 2g; Gash et al. 1996; von Randow et al. 2004; Garcia-Carreras et al. 2010). Otherwise, important and significant changes in the reflected solar radiation are induced by the forest loss. Due to the higher cropland albedo, a general increase in the reflected solar radiation (~ + 2 W m^{-2} or + 5.7%) occurs throughout the year in RegIPSL-Deforested (red line in Fig. 2d) in agreement with measurements from the Anglo-Brazilian Amazonian Climate Observation Study (ABRACOS) project (Berbet and Costa 2003; von Randow et al. 2004). This energy loss, in conjunction with less incoming longwave radiation (− 0.8 W m^{-2} or − 0.17%) due to a drier atmosphere (Fig. 2e–f; Eltahir 1996; Claussen et al. 2001), leads to a reduction in the net surface radiation of ~ − 3 W m^{-2} (− 2.5%) during the dry-to-wet transition season (Fig. 2i). Reductions in the net surface radiation have been reported over cleared areas in the Amazon (Bastable et al. 1993).

4.2 CPs and associated regional composites

Figure 8 shows simulated changes in evapotranspiration for the different atmospheric states or CPs. Similarly, Fig. 9 displays deforestation-induced changes in rainfall and 850 hPa horizontal wind for each CP. At the same time, we use the Taylor diagram for assessing the changes in the spatial patterns of rainfall and horizontal winds for each circulation pattern (Fig. S5). In this case, instead of comparing a reference or 'observed' field with a modeled field as usual, we use the RegIPSL-Control as a reference dataset and evaluate the similarity with the CP spatial distributions in the deforested experiment (RegIPSL-Deforested).

In agreement with our previous results (Sect. 4.1), evapotranspiration decreases over the deforested area mainly in dry and transition regimes (CPs D1, D2, D3, T1 and $T2_{DW}$), driven by reductions in the net surface radiation added to the effect of crop shorter roots (not shown). During these CPs, local weak changes in 850 hPa winds are also registered over the cleared area (Figs. 9 and S6). D1, D2, D3 and T1 exhibit a wind acceleration over the deforested patch associated with a reduced surface roughness length. The stronger winds enhance the surface humidity transport toward central and southwestern Amazon and increase moisture convergence and precipitation in T1 and small patches of $T2_{DW}$ (Figs. 7 and S6). Similar changes in moisture convergence for Amazon deforestation scenarios have been reported in modeling studies (Lean and Rowntree 1997; Eiras-Barca et al. 2020). The slight significant rainfall increases in T1 and $T2_{DW}$ explain the modest, but not significant, precipitation increment over the southern Amazon between October–November shown in previous subsections (see Fig. 2a). On the contrary, a wind deceleration occurs in the deforestation scenario for $T2_{DW}$ over the deforested patch, which is related to a slight increase in moisture convergence (Fig. S6). This is also observed by Ruiz-Vásquez et al. (2020), who identified a weaker southerly cross-equatorial flow during the dry and dry-to-wet transition seasons in association with deforestation over the Southern Amazon. It is important to remark that CP $T2_{DW}$ is an almost exclusive condition of the dry-to-wet transition season and is featured by the encounter of a northerly cross-equatorial flow with southerly wind incursions that generates low-level convergence and triggers precipitation in the southern Amazon and south eastern Brazil (Espinoza et al. 2021). However, a non-statistically significant weakening of the southerly wind incursions below 10°S and between 70°W–50°W is observed with the rainforest loss. It is precisely in this area where cold fronts are frequent during the transition from dry to wet conditions (Machado et al. 2004). A weaker than usual extratropical

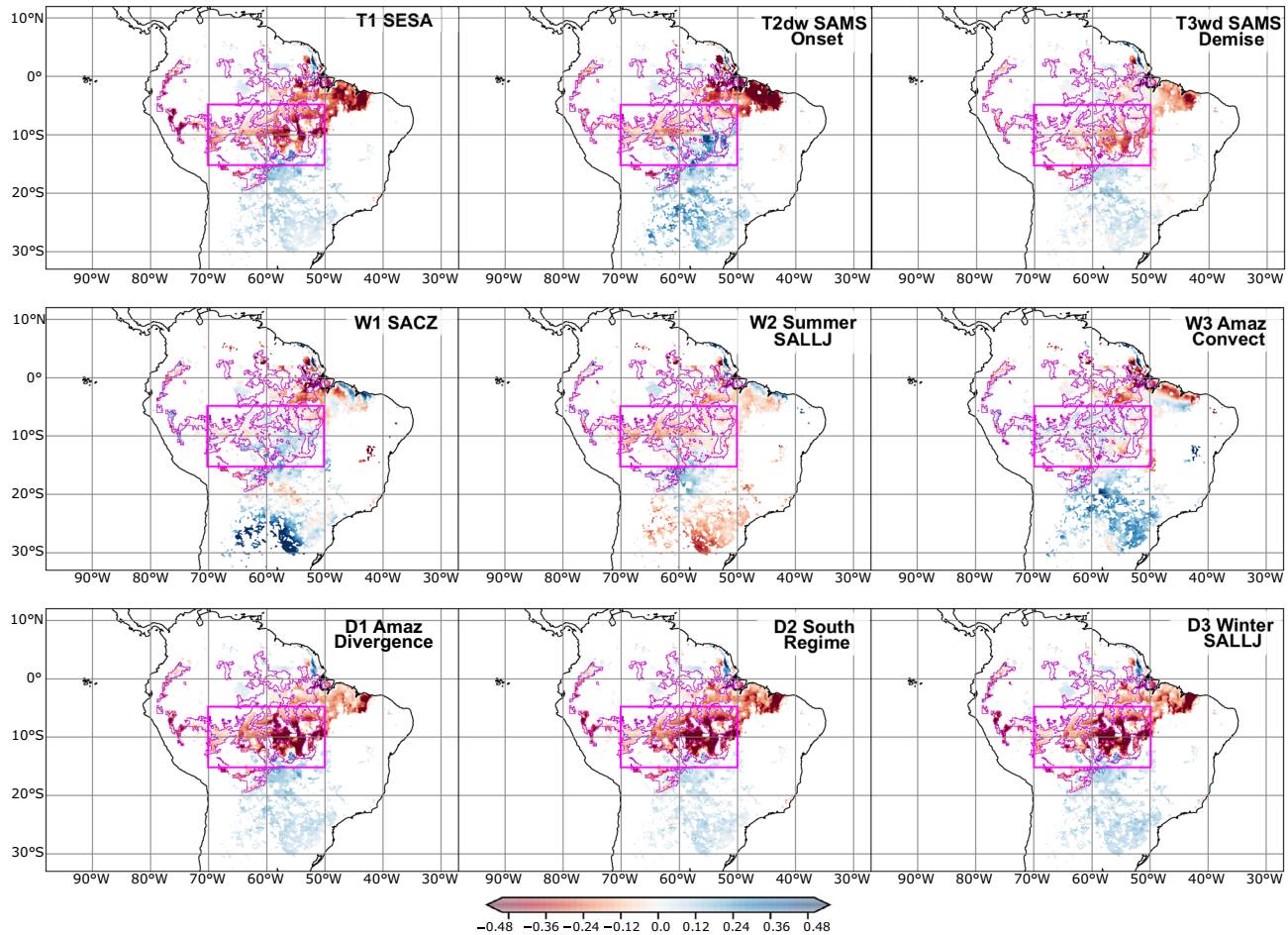

Fig. 8 Differences RegIPSL-Deforested minus RegIPSL-Control in evapotranspiration composites for the 9 circulation patterns (CPs) defined from the k-means clustering analysis. Differences are in mm day^{-1}. Only significant evapotranspiration differences are shown (t-test, $p < 0.05$). Magenta box shows the southern Amazon domain (5°S–15°S, 70°W–50°W). The magenta line highlights the deforested area

cold front incursions are generally related to a delayed rainy season (Li and Fu 2006). Compared with wet season CPs, dry season and transition regimes have almost zero rainfall and wind changes according to Figs. 9, S5 and S6. Minor changes in the regional-scale circulation during the dry season and the dry-to-wet transition period are expected due to the important role of the extratropical forcing in this time of the year (e.g. Jones and Simmonds 1993; Sinclair 1995; Espinoza et al. 2012). In addition, since our simulations are done with a regional climate model laterally forced by ERA5, the deforestation impacts on the atmospheric dynamics are limited to the modeling domain while any external forcing (such as the extratropical westerly Rossby waves) remains undisturbed (Sud et al. 1996; Gedney and Valdes 2000; Badger and Dirmeyer 2016).

During the wet season, the continental thermodynamics and the vegetation role are determinant to shape the regional-scale circulation (e.g. Gill 1980; Figueroa et al. 1995; Eltahir 1996; Gedney and Valdes 2000). Accordingly, deforestation generates profound alterations in the atmospheric circulation and rainfall during this season over the entire continent (Fig. 9). It is in the wet season CPs when the differences in low-level circulation are highest. Thus, lower spatial correlations between RegIPSL- Control and RegIPSL-Deforested are observed for CPs W1–W2–W3 in Fig. S5b, c. The first wet season circulation pattern W1 experiments a weakening of the characteristic circulation of the SACZ (see Table 3 and Fig. 4). Southerly winds are diminished south of 10° S, which allows northerly winds to reach further south and decrease their eastward deviation over the southern Amazon. As a consequence, rainfall is reduced (increased) over the eastern (southern) part of the continent and over the southern Amazon (Fig. 9). A weakened SACZ has been documented in tropical deforestation

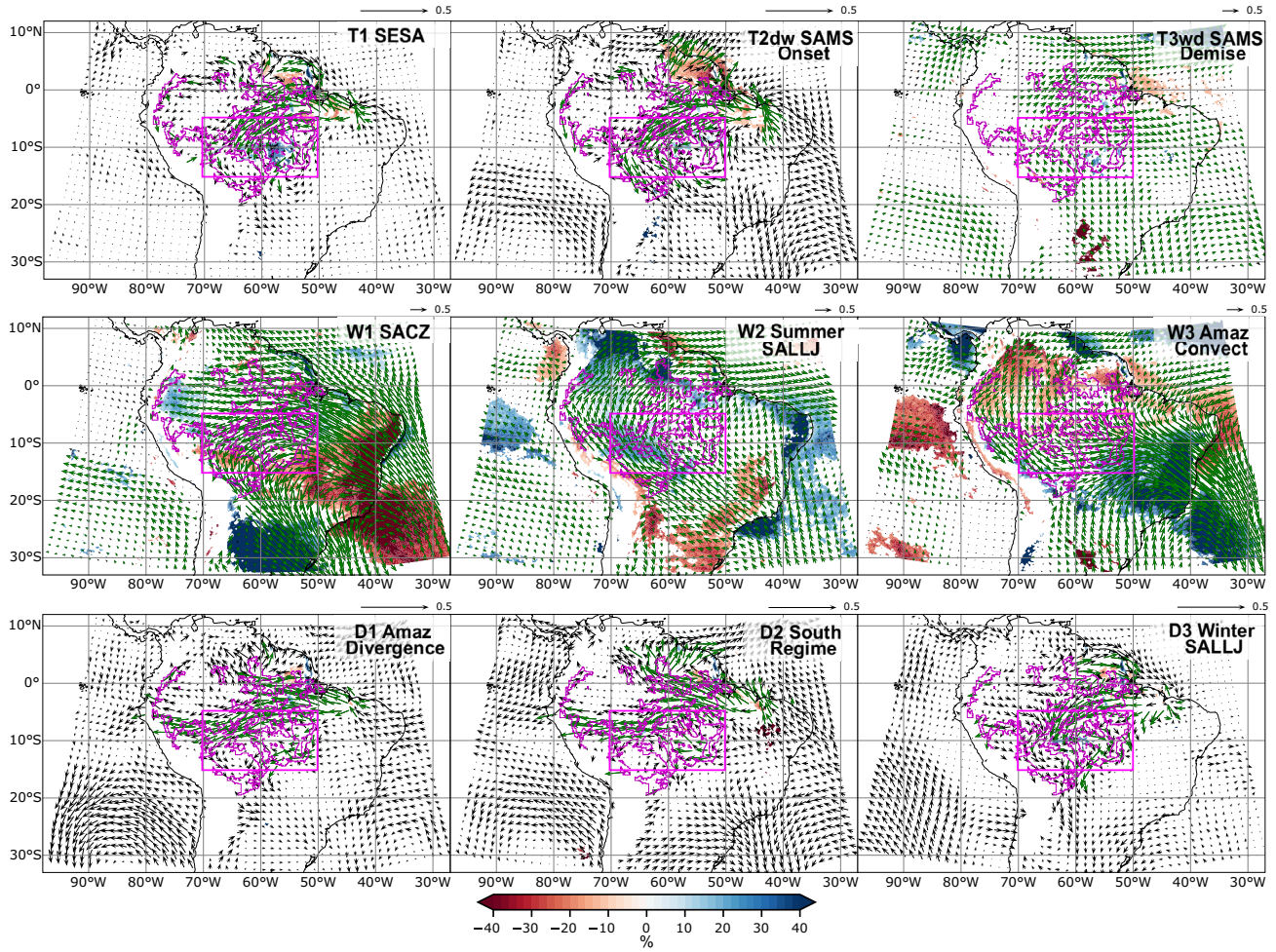

Fig. 9 Differences RegIPSL-Deforested minus RegIPSL-Control in 850 hPa horizontal winds and rainfall composites for the 9 circulation patterns (CPs) defined from the k-means clustering analysis. Rainfall differences (shaded) are in percentage respect to values in the control scenario. Horizontal winds at 850 hPa (vectors) are in m/s. Only significant rainfall differences are shown (t-test, $p < 0.05$). Green vectors represent significant wind differences (t-test, $p < 0.05$). Magenta box shows the southern Amazon (5°S–15°S, 70°W–50°W). The magenta line highlights the deforested area

experiments by previous studies (Badger and Dirmeyer 2016). Similarly, there is a weakening of the northerly winds that feature the summer SALLJ in W2 (Fig. 9). The weaker north–south moisture transport in the deforestation scenario prompts precipitation and moisture convergence increase (decrease) over northern (southern) tropical South America (Figs. 9 and S6). As a component of the SAMS and the summer regional Hadley cell, a weakening of the SALLJ is consistent with deforestation theoretical frameworks and with climate model experiments (Zhang et al. 1996; Eltahir 1996; Zeng and Neelin 1999; Badger and Dirmeyer 2016; Sierra et al. 2021). Finally, W3 displays an enhanced northerly and southerly winds, a stronger eastward deviation and moisture convergence, triggering more convection over southeastern Brazil (Figs. 9 and S6). Changes in low-level winds for W3 are very similar to the normal conditions of W1 (Figs. 4 and 9). In fact, we find that under the deforestation scenario, the days with W1 conditions tend to convert to CP W3 (not shown).

Alterations in the frequency of occurrence for the different CPs in the deforested experiment are shown in Fig. 10. Each subpanel represents the annual cycle frequency for a specific atmospheric regime in RegIPSL-Control and RegIPSL-Deforested (blue and red lines, respectively). In order to assess the statistical significance of the differences in CP frequencies between control and deforested experiments, we implement a bootstrap-like methodology. We split our complete time series for both experiments, using the selected day-to-day classification (see Sect. 2.4), in 10-year running windows. For each time window we compute the frequency of occurrence of each CP in order to get the frequency variance in control and deforestation scenarios. Days with significant differences are highlighted with red dots (p-value < 0.05, Fig. 10).

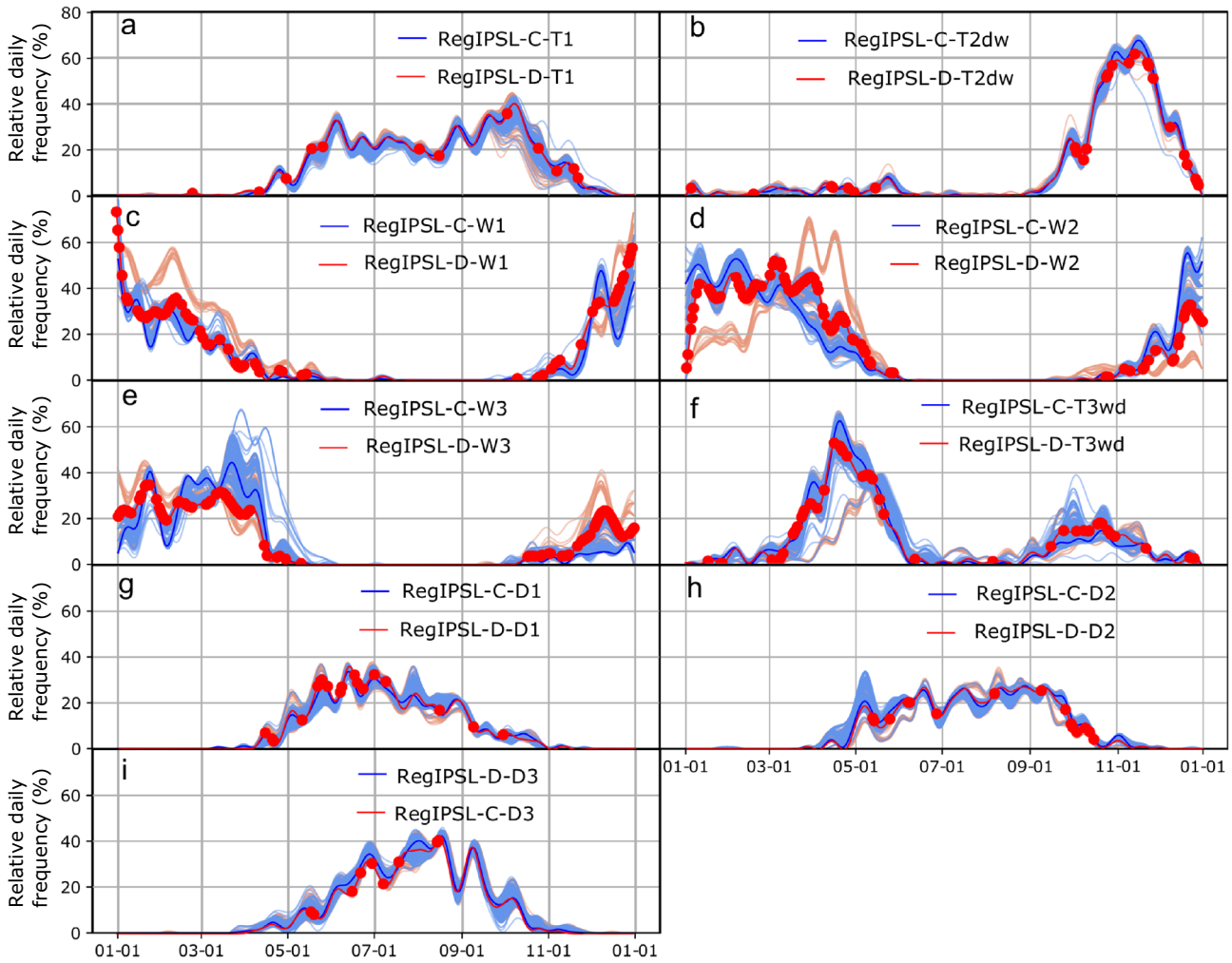

Fig. 10 Relative mean daily frequency of the 9 circulation patterns (CPs, **a-i**) defined from the k-means clustering analysis for RegIPSL-Control ('RegIPSL-C') and RegIPSL-Deforested ('RegIPSL-D'), blue and red lines, respectively. Light blue and red lines correspond to 1000 day-reclassifications with random cluster center initialization in control and deforested scenarios. Solid blue and red lines are the selected partitions for previous section analysis and correspond to a smart selection of initial centroids seeds for k-means. The horizontal axis represents the days from January 1st to December 31st in the climatology during the period 2001–2019. CP's annual cycles were smoothed using a temporal lowpass Butterworth filter retaining only frequencies lower than 1/30 cycles per day

Consistent with our previous results discussed above, transitional CP T1 and dry season CPs D1–D2–D3 experience minor changes in frequency throughout the year with deforestation (Fig. 10a and g–i). Nonetheless, during the dry-to-wet transition period (end of September and October) there is a reduction of − 6% in the frequency of $T2_{DW}$ (Fig. 10b). At the same time, $T3_{WD}$ increases its occurrence in the deforestation experiment by about + 5% (Fig. 10f). As we discussed before, the first atmospheric regime that appears during the wet season corresponds to the SACZ conditions (W1; Fig. 10c). Deforestation induces a decrease in the frequency of W1 at the very beginning of the wet season (− 17%) and an increase between December-February (+ 18%). The decrease in the activity of W1 during this month is linked to the increase in the frequency of W3, reflecting the W1-to-W3 switch discussed before. For the control run, the development of CP W1 is followed by the emergence of the SALLJ (CP W2), conforming the SACZ-SALLJ dipole. However, forest loss alters the development of the SAMS and causes a delay in the W2 activity, with fewer events during November-February (between − 10 to − 20%, depending of the month) and more occurrences at the end of the wet season (March–April; + 10% to + 20% according to the month; Fig. 10d). At the end of the rainy season, between March–April, W3 becomes less frequent and is replaced by W2 events. Similarly, as a consequence of the delayed activity of the SALLJ (W2), $T3_{WD}$ frequency is reduced during late April.

In summary, the changes in $T2_{DW}$, $T3_{WD}$, W1 and W2 point in the same direction: a later onset of the rainy season

based on CPs under the deforested experiment. However, we did not find any change in the onset/end wet season dates using the rainfall-based criteria of Li and Fu (2004). A possible explanation for this is the dependence of this methodology on precipitation, and therefore on the convection parameterization. In agreement with our results, several modeling studies find a more frequent longer dry seasons with the Amazon forest removal (Costa and Pires 2010; Boisier et al. 2015; Nobre et al. 2016; Alves et al. 2017; Ruiz-Vásquez et al. 2020; Commar et al. 2023). Widespread deforestation generates a less heterogenous land cover over southern Amazonia, what can weaken the combined effect of warmer surface, reduced CINE and shallow ascending motion over croplands and the large CAPE available for exploiting these thermally driven vertical wind anomalies over forested areas, thus delaying the large-scale triggering of convection and the wet season onset.

4.3 Analysis of the isolated effect of the CP changes in frequency and characteristic rainfall

Precipitation during the dry-to-wet transition period is crucial for increasing the evapotranspiration, the atmospheric moisture and for triggering shallow convection during the early stages of the rainy season onset (see Sect. 3.4; Wright et al. 2017). Deforestation can alter the rainfall and evapotranspiration during the pre-onset period, and, therefore, impact the whole development of the wet season (Li and Fu 2004). In the previous section we analyze the changes induced by the forest loss in the mean rainfall amount or characteristic rainfall of each circulation pattern, as well as changes on its frequency of occurrence separately. To complement these analyses, the question addressed in this subsection is how these alterations act together to impact the pre-onset rainfall. Therefore, we estimate the relative importance of the changes in CP frequency versus alterations in CP characteristic rainfall induced by deforestation for the total accumulated pre-onset rainfall. Here, the pre-onset period is defined as the 120 days preceding the rainy season onset.

The accumulated rainfall at grid-cell j between the day -120 and the onset (day 0) P_j can be estimated through a decomposition of the characteristic rainfall $p_{j,k}$ associated to each k circulation pattern at location j, multiplied by its frequency of occurrence of during the day i, denoted as $n_{i,k}$, according to Eq. 2.

$$P_j = \sum_{k=1}^{9} \sum_{i=-120}^{0} p_{j,k} n_{i,k} \tag{2}$$

With this approximation, we assume that all the days with atmospheric conditions corresponding to each CP k will have the same associated rainfall, which corresponds to the CP's rainfall composite mean. A similar approach has been previously used for analyzing rainfall variability over different regions (Polcher 1995; Moron et al. 2008). In order to test our approximation, Fig. 11 shows the comparison between the climatology of the accumulated precipitation during the pre-onset period in RegIPSL-Control, and the total rainfall estimation using Eq. 2, labeled as 'reconstruction' (Fig. 11a and b, respectively). The pre-onset period usually occurs between boreal summer and fall (July–September). For this reason, we observe high amounts of accumulated rainfall over northern South America and the Pacific and Atlantic Intertropical Convergence Zone (ITCZ; Fig. 11a). The reconstruction of total rainfall is very close to the accumulated rainfall climatology in spatial structure and rainfall magnitude (Fig. 11b). Precipitation is overestimated by the reconstruction over most of the area (Fig. 11c). Rainfall distribution at daily time scale is usually skewed due to the presence of very frequent zero or non-rainfall values mainly during the dry and dry-to-wet seasons. However, Eq. 2 uses the precipitation probability for each CP computed over the whole year. Therefore, the mean daily precipitation associated with each CP is influenced by precipitation during both rainy and dry seasons while our reconstruction is limited to a relatively dry period. Nevertheless, within our region of interest (southern Amazonia, magenta box in Fig. 11c), the total rainfall overestimation is only about + 70.25 mm (+ 22%) in the three-month period (Fig. 11c). We also compute the reconstruction of the total pre-onset rainfall for the deforestation experiment using the same methodology, in order to evaluate the changes caused by the forest-loss.

Following Eq. 2, we can analyze the deforestation-induced change in total accumulated pre-onset rainfall, as well as the individual effect of the changes in frequency and characteristic rainfall of the CPs. The change in the total pre-onset rainfall at grid-cell j between the deforestation and control experiments dP_j, can be divided in two different terms: (1) a first term representing the effect of changes only in the frequency of each circulation pattern k with deforestation during each day i in the pre-onset period ($dn_{i,k}$). The characteristic rainfall of CP k, $p_{j,k}$, remains unperturbed; (2) a second term corresponding to the effect of changes in the characteristic rainfall of each circulation pattern k, $dp_{j,k}$. This term uses the CP frequencies of occurrence of from the control experiment $n_{i,k}$ (Eq. 3).

$$dP_i = \sum_{k=1}^{9} \sum_{i=-120}^{0} p_{j,k} dn_{i,k} + \sum_{k=1}^{9} \sum_{i=-120}^{0} n_{i,k} dp_{j,k} \tag{3}$$

Figure 11d displays differences in the total pre-onset rainfall reconstructions between the deforested and control experiments. Deforestation increases rainfall over the northern part of the continent (Colombia and Venezuela),

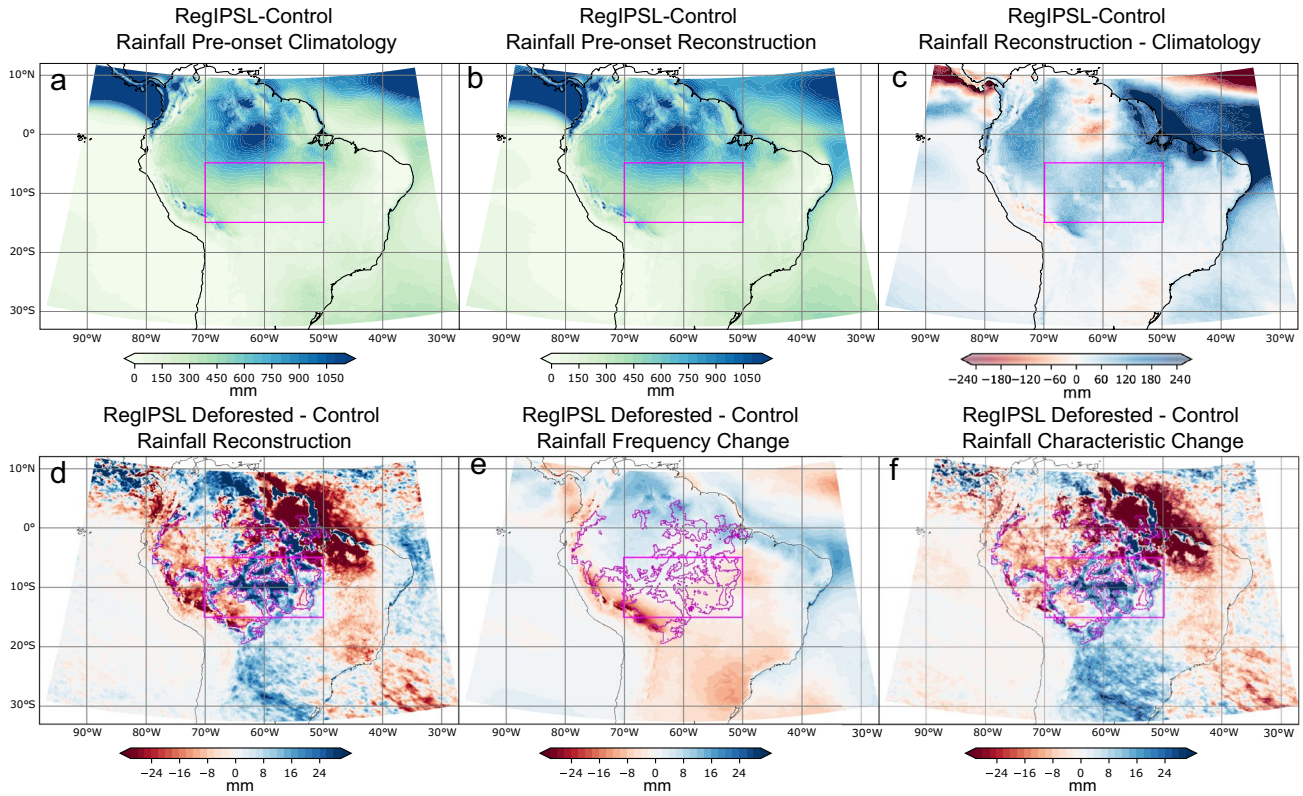

Fig. 11 Total accumulated rainfall for the pre-onset period (day − 120 to day 0 or onset of the rainy season) for: **a** RegIPSL Control climatology and **b** rainfall reconstruction using Eq. 2. **c** Differences in the total accumulated rainfall for the pre-onset period between RegIPSL-Control climatology minus RegIPSL reconstruction. **d** Differences in the total accumulated rainfall between reconstructions in the RegIPSL-Deforested minus RegIPSL-Control experiment. **e** Total accumulated rainfall changes induced by deforestation due to alterations in the frequency of the circulation patterns. **f** Total accumulated rainfall changes induced by deforestation due to alterations in the characteristic rainfall of the circulation patterns. Magenta box shows the southern Amazon (5°S–15°S, 70°W–50°W). The magenta line highlights the deforested area. All subplots are in mm

the southeastern South America (La Plata basin) and over the deforested areas of central and southern Amazon. On the other hand, rainfall decreases over the eastern flank of the Andes, the northeastern Atlantic coast, southeastern Brazil and over the surrounding areas of the deforested patches. Over the southern Amazon, rainfall increases on average by + 2.98 mm. This rainfall increment is confined over the cleared areas (+ 12.17 mm), whereas over non-deforested areas rainfall decreases around − 5.43 mm. This enhanced rainfall over deforested patches and its reduction over forested neighboring areas is a typical spatial structure of the observed local thermally-driven circulations induced by deforestation during the Amazonian dry season (Souza et al. 2000; Negri et al. 2004; Chagnon and Bras 2005; Wang et al. 2009).

Changes in the regional total pre-onset precipitation due to the alterations in the CPs frequency exhibit a very different spatial pattern. A latitudinal dipole with more (less) rainfall in the northern (southern) part of the continent is observed (Fig. 11e). It is interesting to note that the local precipitation changes over the deforested patches observed in the differences between deforested and control pre-onset rainfall climatology are not explained by the alteration in the CPs frequency. Conversely, changes in the frequency of occurrence generate a regional-scale rainfall response. Precipitation reduction over the eastern flank of the Andes (Fig. 11d) is almost completely explained by the alteration of CPs frequency. During the pre-onset period, the most frequent CPs are the dry season regimes D1–D2–D3 and transitional CPs T1 and T2dw (see Sect. 3.3). However, deforestation affects mostly the frequency of CP T2dw (reduces its frequency in about − 6%) while the rest of the weather regimes do not exhibit significant changes (see Sect. 4.2). For this reason, the isolated effect of CP frequency changes on the total pre-onset rainfall is very similar to a negative phase of the rainfall anomalies linked to the CP T2wd (see Fig. 4). Under normal conditions, during this period of the year, the southern Amazon receives precipitation due to the activity of the CP T2dw. Thus, it is expected that a reduction in the occurrence of T2dw generates a rainfall decrease of

− 2.48 mm over the southern Amazon. This rainfall reduction occurs over both deforested and non-deforested areas (− 1.71 mm and − 3.18 mm, respectively) as it is related to regional circulation changes.

Alterations in the CPs characteristic rainfall induced by deforestation dominate the total change in the accumulated pre-onset precipitation over most of the region (Fig. 11d–f). The precipitation increase over the deforested areas and the decrease over the surroundings is fully explained by the changes in the CP's characteristic rainfall. In this way, the local effects of deforestation seem to influence the magnitude and spatial distribution of rainfall associated with each CP rather than its frequency. However, rainfall alterations over the SESA-SACZ region suggest that deforestation also generates a regional-scale effect outside the deforested area boundaries in the rainfall pattern linked with each CP. As our results were obtained using a regional climate model with imposed large-scale circulation at the boundaries of the spatial domain, the regional rainfall changes induced by alterations in the CP frequencies should be confirmed by using a global climate model which fully represents the non-local effects of the Amazonian forest loss (Zhang et al. 1996; Gedney and Valdes 2000). Conversely to the southern Amazon rainfall depletion linked to the changes in the CPs frequency, changes in the characteristic CPs rainfall cause a rainfall increase of + 5.48 mm. This rainfall increase is observed over the deforested areas (+ 13.94 mm) as a local response to forest loss. At the same time, rainfall is decreased (− 2.24 mm) over the neighboring non-cleared areas as a result of the development of mesoscale circulations supported by thermal contrast due to land surface heterogeneities (Souza et al. 2000; Wang et al. 2009; Wongchuig et al. 2023 submitted to Journal of Hydrology).

5 Summary and conclusions

Previous works suggest that tropical rainforest evapotranspiration is crucial moistening the lower troposphere, for triggering shallow convection and for initiating the wet season onset (Li and Fu 2004; Wright et al. 2017). However, how deforestation can affect the initiation of the Amazon wet season is something that remains poorly understood. In this study, we assess the impacts of the Amazon forest-to-cropland conversion on the climatic conditions during the dry-to-wet transition period (August–September), as well as on the onset and development of the rainy season in the southern Amazon (5°S–15°S, 70°W–50°W). Using a weather typing approach, we decompose the atmospheric circulation variability in tropical South America in its dominant modes in order to analyze perturbations induced by deforestation in the evolution of the rainy season. To accomplish this, we use 19 years of simulations (2001–2019) with the regional climate model RegIPSL under two scenarios: (1) a control scenario and (2) a deforestation scenario based on future projections of Amazonian forest loss developed by Soares-Filho et al. (2006).

The validation of the model is performed in three steps. First, the representation of the annual cycle in water and energy variables over the southern Amazon is evaluated. By comparing with satellite, *in-situ* measurements and reanalysis data, we find a well-represented seasonality of precipitation, evapotranspiration and surface energy fluxes by RegIPSL-Control. Using ERA5 horizontal winds at 850 hPa, the atmospheric low-level circulation variability is decomposed in 9 regimes that correspond to recurrent atmospheric states or circulation patterns (CPs). As previous works, we identify three dry season (D1–D2–D3), three wet season (W1–W2–W3) and three transitional ($T1–T2_{DW}–T3_{WD}$) regimes (Espinoza et al. 2021). Therefore, in the second validation step we assess the model's skill to properly represent the spatial structure and the relative frequency of each CP along the year. A direct comparison with ERA5/CHIRPS wind and rainfall anomalies shows that RegIPSL-Control reproduces broadly the main atmospheric circulations and its seasonality. Finally, we complement the validation analyzing the evolution in the atmospheric and surface conditions during the preceding and subsequent days of the wet season onset. Despite small differences, RegIPSL-Control is able to represent a realistic time evolution of the atmospheric circulation, rainfall and evapotranspiration in the preceding and subsequent days of the wet season onset, what enables the use of this model for exploring deforestation changes in the evolution of the dry-to-wet transition.

The southern Amazon is a region with land cover heterogeneity (mainly forest and cropland/grassland). Different vegetation types can play a distinct role in the development of the wet season onset. Thus, we use outputs from the control experiment to analyze the differential behavior of forest and croplands/grasslands along the preceding and subsequent days of the rainy season onset. The temporal evolution of surface and atmospheric variables is similar over crop/grass and forest areas and is controlled by large-scale phenomena. Nevertheless, the magnitude of the forest and croplands/grasslands response to the synoptic forcing is different before the onset of the rainy season. Less rainfall is simulated by RegIPSL-Control over croplands/grasslands until wet season CPs W1–W2 begin to occur. Although the forest areas exhibit higher evapotranspiration rates during the pre-onset period, crops respond rapidly to the first rainy events before the wet season onset, and by the onset date, crops and forest present similar evapotranspiration values. Due to the higher evapotranspiration rates, the atmospheric column above forest areas is moister and contain more convective available potential energy (CAPE) before the

onset. However, crop/grass areas present a warmer low-level atmosphere as a consequence of higher sensible heat flux. Consequently, the lower troposphere is destabilized over croplands/grasslands developing a shallow ascending motion during the beginning of the wet-to-dry transition season. Crop/grass low-level ascending motion is suppressed by large-scale subsidence associated to dry season CPs until 50 days before the onset. By this time, the locally forced ascension overcomes the regional subsidence and generates deep convection in the region, mainly over rainforest areas, where the atmosphere presents higher potential for triggering convection. Finally, with the wet season onset, the different response of forest and croplands/grasslands to the synoptic forcing vanishes, and both vegetation type behave similarly to the regional atmospheric conditions.

With respect to our analysis on the impact of deforestation over the southern Amazon, deforestation increases the reflected solar radiation, and decreases net surface radiation, evapotranspiration and latent heat flux during the dry and dry-to-wet seasons. Dry season atmospheric regimes D1-D2-D3 suffer very local changes in circulation, with a wind acceleration over the deforested areas linked to a reduction in the surface roughness length. Additionally, deforestation does not affect the frequency of occurrence of dry season atmospheric regimes D1–D2–D3 or the transitional circulation pattern T1. It is only by the end of the pre-onset period, when important changes in circulation and frequency of occurrence begin to be important. The CP T2wd, which characterizes the atmospheric conditions during the onset of the rainy season over the southern Amazonia, decreases its frequency of occurrence in about − 6% with deforestation suggesting a delayed wet season onset. Changes in the atmospheric circulation patterns linked to the SACZ and the SALLJ reinforce the idea of a deforestation-induced dry season lengthening in agreement with previous studies (Costa and Pires 2010; Boisier et al. 2015; Nobre et al. 2016; Alves et al. 2017; Ruiz-Vásquez et al. 2020; Douville et al. 2021; Commar et al. 2023). Additionally, the austral summer SALLJ experiments a weakening of the northerly winds that transport moisture toward southern South America in the deforestation scenario, which increases (decreases) precipitation in the northern (southern) part of the continent.

Finally, during the 120 days preceding the rainy season onset (pre-onset period), deforestation induces a rainfall increase over the northern and southeastern parts of the South American continent, as well as over the deforested patches of the central and southern Amazon (+ 12.17 mm). At the same time, precipitation is decreased over the eastern flank of the Andes, the northeastern Atlantic coast, and over the forested areas in the vicinity of the deforested patches (− 5.43 mm). Through a decomposition of the individual attribution of changes in frequency and changes in the CP characteristic associated rainfall, we identify two opposite effects on the accumulated pre-onset rainfall: (1) a more regional deforestation-induced change linked to a rainfall decrease (increase) over the southern (northern) part of the continent and the eastern flank of the Andes. This change is caused solely by changes in the frequency of the CPs, mainly by the reduced occurrence of the T2dw; (2) a combination of local and regional rainfall responses linked to perturbations in the CP's associated rainfall. The local signal explains the precipitation increase (decrease) over the deforested areas (the surroundings of the deforested areas), while the regional part is related with the rainfall rise over the southeastern South America.

Based on a weather typing approach, and therefore on the representation of the atmospheric circulation from daily to inter-decadal timescales, our results strengthen the link between the deforestation and the lengthening of the dry season over the southern Amazonia. At the same time, these results show how the impacts of deforestation are not limited to the wet season onset and affect the main features of circulation patterns during the dry-to-wet season. In fact, we conclude that the land–atmosphere interactions show differentiated changes through the year. Local alterations near the land surface dominate during the dry and dry-to-wet transition seasons, while regional-scale changes in the atmospheric circulation and precipitation are observed during the wet season. However, the physical mechanisms behind the changes in the frequency and spatial structure of wet season circulation patterns remain unexplored in the present work. As far as we know, this is one of the few works analyzing the effect of deforestation on the evolution of the rainy season at intra-seasonal timescales instead of looking for seasonal changes. Understanding the progress of deforestation perturbations on the regional atmospheric circulation is crucial in order to better comprehend the forest role on the climate system at different timescales.

Supplementary Information The online version contains supplementary material available at https://doi.org/10.1007/s00382-023-06835-2.

Acknowledgements This research has been supported by the French AMANECER-MOPGA project funded by ANR and IRD (ANR-18-MPGA-0008), and by the ACE-Amazon project funded by the regional program CLIMAT-AmSud (21-CLIMAT-01). MINCyT-ECOS Sud ref. A18D04 (Argentina-France) and INSU LEFE ref. 12962 are also acknowledged. At the same time, this work was granted access to the HPC resources of IDRIS under the allocation 2021-101054 made by GENCI. Simulations were run on the Jean Zay HPC at the French computing center IDRIS. The authors would also like to thank the following agencies/organizations for providing access to data: The Climate Hazards Group Infrared Precipitation for providing CHIRPS, Paca, V. H. d. M. (2019) for providing ET-Amazon and the Copernicus Climate Change Service (C3S) for providing horizontal wind fields and surface fluxes from ERA5 and ERA5-Land. Anthony Schrapffer was funded by PICT 2014-0887, PICT-2015-3097, PICT-2017-1406 (ANPCyT, Argentina). Paola A. Arias was funded by MINCIENCIAS through the grant No. 80740-490-2020.

Author contributions All authors contributed to the study conception and design. Material preparation, data collection and analysis were performed by JPS. The first draft of the manuscript was written by JPS and all authors commented on previous versions of the manuscript. All authors read and approved the final manuscript.

Funding This research has been supported by the French AMANECER-MOPGA project funded by ANR and IRD (ANR-18-MPGA-0008), and by the ACE-Amazon project funded by the regional program CLIMAT-AmSud (21-CLIMAT-01). At the same time, this work was granted access to the HPC resources of IDRIS under the allocation 2021-101054 made by GENCI. Anthony Schrapffer was funded by PICT 2014-0887, PICT-2015-3097, PICT-2017-1406 (ANPCyT, Argentina). Paola A. Arias was funded by MINCIENCIAS through the grant No. 80740-490-2020.

Data availability All dataset sources, except RegIPSL modeling results, have been properly referenced by showing the source (web site links). The datasets generated during the current study (RegIPSL outputs) are available from the corresponding author on reasonable request.

Declarations

Conflict of interest The authors have no relevant financial or non-financial interests to disclose.

References

Adler B, Kalthoff N, Gantner L (2011) Initiation of deep convection caused by land-surface inhomogeneities in West Africa: a modelled case study. Meteorol Atmos Phys 112:15–27. https://doi.org/10.1007/s00703-011-0131-2

Agudelo J, Arias PA, Vieira SC, Martínez JA (2019) Influence of longer dry seasons in the Southern Amazon on patterns of water vapor transport over northern South America and the Caribbean. Clim Dyn 52:2647–2665. https://doi.org/10.1007/s00382-018-4285-1

Alves LM, Marengo JA, Fu R, Bombardi RJ (2017) Sensitivity of Amazon regional climate to deforestation. Am J Clim Chang. https://doi.org/10.4236/ajcc.2017.61005

Arias PA, Fu R, Vera C, Rojas M (2015) A correlated shortening of the North and South American monsoon seasons in the past few decades. Clim Dyn 45:3183–3203. https://doi.org/10.1007/s00382-015-2533-1

Arias PA, Martínez JA, Mejía JD et al (2020) Changes in normalized difference vegetation index in the Orinoco and Amazon River basins: links to tropical Atlantic surface temperatures. J Clim 33:8537–8559. https://doi.org/10.1175/JCLI-D-19-0696.1

Arias P, Bellouin N, Coppola E, et al (2021) Climate Change 2021: the physical science basis. Contribution of Working Group14 I to the Sixth Assessment Report of the Intergovernmental Panel on Climate Change; Technical Summary. Cambridge University Press

Asner GP (2009) Tropical forest carbon assessment: integrating satellite and airborne mapping approaches. Environ Res Lett 4:034009. https://doi.org/10.1088/1748-9326/4/3/034009

Badger AM, Dirmeyer PA (2016) Remote tropical and sub-tropical responses to Amazon deforestation. Clim Dyn 46:3057–3066. https://doi.org/10.1007/s00382-015-2752-5

Bagley JE, Desai AR, Harding KJ et al (2014) Drought and deforestation: has land cover change influenced recent precipitation extremes in the Amazon? J Clim 27:345–361. https://doi.org/10.1175/JCLI-D-12-00369.1

Baker JCA, Spracklen DV (2019) Climate benefits of intact amazon forests and the biophysical consequences of disturbance. Front For Glob Chang. https://doi.org/10.3389/ffgc.2019.00047

Ban N, Caillaud C, Coppola E et al (2021) The first multi-model ensemble of regional climate simulations at kilometer-scale resolution, part I: evaluation of precipitation. Clim Dyn 57:275–302. https://doi.org/10.1007/s00382-021-05708-w

Barichivich J, Gloor E, Peylin P et al (2018) Recent intensification of Amazon flooding extremes driven by strengthened Walker circulation. Sci Adv. https://doi.org/10.1126/sciadv.aat8785

Bastable HG, Shuttleworth WJ, Dallarosa RLG et al (1993) Observations of climate, albedo, and surface radiation over cleared and undisturbed amazonian forest. Int J Climatol. https://doi.org/10.1002/joc.3370130706

Berbet MLC, Costa MH (2003) Climate change after tropical deforestation: seasonal variability of surface Albedo and its effects on precipitation change. J Clim 16:2099–2104. https://doi.org/10.1175/1520-0442(2003)016%3c2099:CCATDS%3e2.0.CO;2

Boisier JP, Ciais P, Ducharne A, Guimberteau M (2015) Projected strengthening of Amazonian dry season by constrained climate model simulations. Nat Clim Chang 5:656–660. https://doi.org/10.1038/nclimate2658

Bonan GB (2008) Forests and climate change: forcings, feedbacks, and the climate benefits of forests. Science 320(5882):1444–1449. https://doi.org/10.1126/science.1155121

Bontemps S, Defourny P, Radoux J, et al (2013) Consistent global land cover maps for climate modelling communities: current achievements of the ESA land cover CCI. In: Proceedings of the ESA living planet symposium. Edimburgh, pp 9–13

Brienen RJW, Phillips OL, Feldpausch TR et al (2015) Long-term decline of the Amazon carbon sink. Nature 519:344–348. https://doi.org/10.1038/nature14283

Butt N, De Oliveira PA, Costa MH (2011) Evidence that deforestation affects the onset of the rainy season in Rondonia, Brazil. J Geophys Res Atmos. https://doi.org/10.1029/2010JD015174

Caioni C, Silvério DV, Macedo MN et al (2020) Droughts amplify differences between the energy balance components of amazon forests and croplands. Remote Sens 12:525. https://doi.org/10.3390/rs12030525

Calinski T, Harabasz J (1974) A dendrite method for cluster analysis. Commun Stat—Theory Methods 3:1–27. https://doi.org/10.1080/03610927408827101

Case JL, Crosson WL, Kumar SV et al (2008) Impacts of high-resolution land surface initialization on regional sensible weather forecasts from the WRF model. J Hydrometeorol 9:1249–1266. https://doi.org/10.1175/2008JHM990.1

Cerón WL, Molina-Carpio J, Ayes Rivera I et al (2020) A principal component analysis approach to assess CHIRPS precipitation dataset for the study of climate variability of the La Plata Basin, Southern South America. Nat Hazards 103:767–783. https://doi.org/10.1007/s11069-020-04011-x

Chagnon FJF, Bras RL (2005) Contemporary climate change in the Amazon. Geophys Res Lett 32:L13703. https://doi.org/10.1029/2005GL022722

Chen Y, Randerson JT, Morton DC et al (2011) Forecasting fire season severity in South America using sea surface temperature anomalies. Science (80-) 334:787–791. https://doi.org/10.1126/science.1209472

Claussen M, Brovkin V, Ganopolski A (2001) Biophysical versus biogeochemical feedbacks of large-scale land cover change. Geophys Res Lett. https://doi.org/10.1029/2000GL012471

Cochrane MA, Alencar A, Schulze MD et al (1999) Positive feedbacks in the fire dynamic of closed canopy tropical forests. Science (80-) 284:1832–1835. https://doi.org/10.1126/science.284.5421.1832

Coe MT, Costa MH, Soares-Filho BS (2009) The influence of historical and potential future deforestation on the stream flow of the Amazon River—land surface processes and atmospheric feedbacks. J Hydrol 369:165–174. https://doi.org/10.1016/j.jhydrol.2009.02.043

Commar LFSA, Abrahão GM, Costa MH (2023) A possible deforestation-induced synoptic-scale circulation that delays the rainy season onset in Amazonia. Environ Res Lett. https://doi.org/10.1088/1748-9326/acc95f

Correa IC, Arias PA, Rojas M (2021) Evaluation of multiple indices of the South American monsoon. Int J Climatol. https://doi.org/10.1002/joc.6880

Cosgrove BA, Lohmann D, Mitchell KE et al (2003) Land surface model spin-up behavior in the North American Land Data Assimilation System (NLDAS). J Geophys Res Atmos 108:2002JD003316. https://doi.org/10.1029/2002JD003316

Costa MH, Pires GF (2010) Effects of Amazon and Central Brazil deforestation scenarios on the duration of the dry season in the arc of deforestation. Int J Climatol 30:1970–1979. https://doi.org/10.1002/joc.2048

Cox PM, Harris PP, Huntingford C et al (2008) Increasing risk of Amazonian drought due to decreasing aerosol pollution. Nature 453:212–215. https://doi.org/10.1038/nature06960

Craig A, Valcke S, Coquart L (2017) Development and performance of a new version of the OASIS coupler, OASIS3-MCT_3.0. Geosci Model Dev 10:3297–3308. https://doi.org/10.5194/gmd-10-3297-2017

Cutrim E, Martin DW, Rabin R (1995) Enhancement of cumulus clouds over deforested lands in Amazonia. Bull Am Meteorol Soc 76:1801–1805. https://doi.org/10.1175/1520-0477(1995)076%3c1801:EOCCOD%3e2.0.CO;2

da Anunciação YMT, Walde DH-G, da Rocha RP (2014) Observed summer weather regimes and associated extreme precipitation over Distrito Federal, west-central Brazil. Environ Earth Sci 72:4835–4848. https://doi.org/10.1007/s12665-014-3607-9

da Paca VH, M, Espinoza-Dávalos GE, Hessels TM et al (2019) The spatial variability of actual evapotranspiration across the Amazon River Basin based on remote sensing products validated with flux towers. Ecol Process 8:6. https://doi.org/10.1186/s13717-019-0158-8

da Silva HJF, Gonçalves WA, Bezerra BG (2019) Comparative analyzes and use of evapotranspiration obtained through remote sensing to identify deforested areas in the Amazon. Int J Appl Earth Obs Geoinf 78:163–174. https://doi.org/10.1016/j.jag.2019.01.015

Da Silveira Lobo Sternberg L (2001) Savanna-forest hysteresis in the tropics. Glob Ecol Biogeogr 10:369–378. https://doi.org/10.1046/j.1466-822X.2001.00243.x

Davidson EA, de Araújo AC, Artaxo P et al (2012) The Amazon basin in transition. Nature 481:321–328. https://doi.org/10.1038/nature10717

de Goncalves LGG, Shuttleworth WJ, Chou SC et al (2006) Impact of different initial soil moisture fields on Eta model weather forecasts for South America. J Geophys Res 111:D17102. https://doi.org/10.1029/2005JD006309

Debortoli NS, Dubreuil V, Funatsu B et al (2015) Rainfall patterns in the Southern Amazon: a chronological perspective (1971–2010). Clim Change 132:251–264. https://doi.org/10.1007/s10584-015-1415-1

Diday E, Simon JC (1976) Clustering analysis, digital pattern recognition. Commun Cybern 10:47–94

Dirmeyer PA, Brubaker KL (2007) Characterization of the global hydrologic cycle from a back-trajectory analysis of atmospheric water vapor. J Hydrometeorol. https://doi.org/10.1175/JHM557.1

Dominguez F, Eiras-Barca J, Yang Z et al (2022) Amazonian moisture recycling revisited using WRF with water vapor tracers. J Geophys Res Atmos. https://doi.org/10.1029/2021JD035259

Douville H, Raghavan K, Renwick J, et al (2021) Water Cycle Changes. In Climate Change 2021: The Physical Science Basis. Contribution of Working Group I to the Sixth Assessment Report of the Intergovernmental Panel on Climate Change [Masson-Delmotte, V., P. Zhai, A. Pirani, S.L. Connors, C. Péan, S. Cambridge University Press, Cambridge, United Kingdom and New York, NY, USA

Eghdami M, Barros AP (2019) Extreme orographic rainfall in the eastern Andes tied to cold air intrusions. Front Environ Sci. https://doi.org/10.3389/fenvs.2019.00101

Eiras-Barca J, Dominguez F, Yang Z et al (2020) Changes in South American hydroclimate under projected Amazonian deforestation. Ann N Y Acad Sci. https://doi.org/10.1111/nyas.14364

Eltahir EAB (1996) Role of vegetation in sustaining large-scale atmospheric circulations in the tropics. J Geophys Res Atmos 101:4255–4268. https://doi.org/10.1029/95JD03632

Eltahir EAB, Bras RL (1994) Precipitation recycling in the Amazon basin. Q J R Meteorol Soc. https://doi.org/10.1002/qj.49712051806

ESA (2017) Land Cover CCI Product User Guide Version 2

Espinoza JC, Guyot JL, Ronchail J et al (2009) Contrasting regional discharge evolutions in the Amazon basin (1974–2004). J Hydrol 375:297–311. https://doi.org/10.1016/j.jhydrol.2009.03.004

Espinoza JC, Lengaigne M, Ronchail J, Janicot S (2012) Large-scale circulation patterns and related rainfall in the Amazon Basin: a neuronal networks approach. Clim Dyn 38:121–140. https://doi.org/10.1007/s00382-011-1010-8

Espinoza JC, Ronchail J, Lengaigne M et al (2013) Revisiting wintertime cold air intrusions at the east of the Andes: propagating features from subtropical Argentina to Peruvian Amazon and relationship with large-scale circulation patterns. Clim Dyn 41:1983–2002. https://doi.org/10.1007/s00382-012-1639-y

Espinoza JC, Ronchail J, Marengo JA, Segura H (2019) Contrasting North–South changes in Amazon wet-day and dry-day frequency and related atmospheric features (1981–2017). Clim Dyn. https://doi.org/10.1007/s00382-018-4462-2

Espinoza JC, Arias PA, Moron V et al (2021) Recent changes in the atmospheric circulation patterns during the dry-to wet transition season in south tropical South America (1979–2020): impacts on precipitation and fire season. J Clim. https://doi.org/10.1175/JCLI-D-21-0303.1

Fassoni-Andrade AC, Fleischmann AS, Papa F et al (2021) Amazon hydrology from space: scientific advances and future challenges. Rev Geophys. https://doi.org/10.1029/2020RG000728

Fearnside PM (1993) Deforestation in Brazilian Amazonia: the effect of population and land tenure. Ambio. https://doi.org/10.1016/0006-3207(94)90222-4

Figueroa SN, Nobre CA (1990) Precipitation distribution over central and western tropical South America. Climanálise 5(6):36–45

Figueroa SN, Satyamurty P, Da Silva Dias PL (1995) Simulations of the summer circulation over the south American region with an Eta coordinate model. J Atmos Sci 52:1573–1584. https://doi.org/10.1175/1520-0469(1995)052%3c1573:SOTSCO%3e2.0.CO;2

Fisch G, Tota J, Machado LAT et al (2004) The convective boundary layer over pasture and forest in Amazonia. Theor Appl Climatol 78:47–59. https://doi.org/10.1007/s00704-004-0043-x

Fisher JB, Whittaker RJ, Malhi Y (2011) ET come home: potential evapotranspiration in geographical ecology. Glob Ecol Biogeogr 20(1):1–18. https://doi.org/10.1111/j.1466-8238.2010.00578.x

Flato G, Marotzke J, Abiodun B, et al (2013) Evaluation of climate models. In: Climate Change 2013: The Physical Science Basis.

Contribution of Working Group I to the Fifth Assessment Report of the Intergovernmental Panel on Climate Change

Fosser G, Khodayar S, Berg P (2015) Benefit of convection permitting climate model simulations in the representation of convective precipitation. Clim Dyn 44:45–60. https://doi.org/10.1007/s00382-014-2242-1

Froidevaux P, Schlemmer L, Schmidli J et al (2014) Influence of the background wind on the local soil moisture-precipitation feedback. J Atmos Sci 71:782–799. https://doi.org/10.1175/JAS-D-13-0180.1

Fu R, Yin L, Li W et al (2013) Increased dry-season length over southern Amazonia in recent decades and its implication for future climate projection. Proc Natl Acad Sci USA. https://doi.org/10.1073/pnas.1302584110

Fu R, Zhu B, Dickinson RE (1999) How do atmosphere and land surface influence seasonal changes of convection in the tropical Amazon? J Clim 12(5):1306–1321. https://doi.org/10.1175/1520-0442(1999)0122.0.CO;2

Funatsu BM, Le Roux R, Arvor D et al (2021) Assessing precipitation extremes (1981–2018) and deep convective activity (2002–2018) in the Amazon region with CHIRPS and AMSU data. Clim Dyn 57:827–849. https://doi.org/10.1007/s00382-021-05742-8

Funk C, Peterson P, Landsfeld M et al (2015) The climate hazards infrared precipitation with stations—a new environmental record for monitoring extremes. Sci Data 2:150066. https://doi.org/10.1038/sdata.2015.66

Gan MA, Kousky VE, Ropelewski CF (2004) The South America monsoon circulation and its relationship to rainfall over west-central Brazil. J Clim 17:47–66. https://doi.org/10.1175/1520-0442(2004)017%3c0047:TSAMCA%3e2.0.CO;2

Garcia-Carreras L, Parker DJ, Taylor CM et al (2010) Impact of mesoscale vegetation heterogeneities on the dynamical and thermodynamic properties of the planetary boundary layer. J Geophys Res 115:D03102. https://doi.org/10.1029/2009JD012811

Gash JHC, Nobre CA (1997) Climatic effects of amazonian deforestation: some results from ABRACOS. Bull Am Meteorol Soc 78:823–830. https://doi.org/10.1175/1520-0477(1997)078%3c0823:CEOADS%3e2.0.CO;2

Gash JHC, Nobre CA, Roberts JM, Victoria RL (1996) Amazonian deforestation and climate. John Wiley, Chichester

Gedney N, Valdes PJ (2000) The effect of Amazonian deforestation on the northern hemisphere circulation and climate. Geophys Res Lett. https://doi.org/10.1029/2000GL011794

Gill AE (1980) Some simple solutions for heat-induced tropical circulation. Q J R Meteorol Soc 106:447–462

Grell GA, Freitas SR (2014) A scale and aerosol aware stochastic convective parameterization for weather and air quality modeling. Atmos Chem Phys 14:5233–5250. https://doi.org/10.5194/acp-14-5233-2014

Guan K, Pan M, Li H et al (2015) Photosynthetic seasonality of global tropical forests constrained by hydroclimate. Nat Geosci 8:284–289. https://doi.org/10.1038/ngeo2382

Haghtalab N, Moore N, Heerspink BP, Hyndman DW (2020) Evaluating spatial patterns in precipitation trends across the Amazon basin driven by land cover and global scale forcings. Theor Appl Climatol 140:411–427. https://doi.org/10.1007/s00704-019-03085-3

Hersbach H, Bell B, Berrisford P et al (2020) The ERA5 global reanalysis. Q J R Meteorol Soc 146:1999–2049. https://doi.org/10.1002/qj.3803

Hoffmann L, Günther G, Li D et al (2019) From ERA-Interim to ERA5: the considerable impact of ECMWF's next-generation reanalysis on Lagrangian transport simulations. Atmos Chem Phys 19:3097–3124. https://doi.org/10.5194/acp-19-3097-2019

Horel JD, Hahmann AN, Geisler JE (1989) An investigation of the annual cycle of convective activity over the tropical Americas. J Clim 2:1388–1403. https://doi.org/10.1175/1520-0442(1989)002%3c1388:AIOTAC%3e2.0.CO;2

Hutyra LR, Munger JW, Nobre CA et al (2005) Climatic variability and vegetation vulnerability in Amazônia. Geophys Res Lett 32:L24712. https://doi.org/10.1029/2005GL024981

Iacono MJ, Delamere JS, Mlawer EJ et al (2008) Radiative forcing by long-lived greenhouse gases: Calculations with the AER radiative transfer models. J Geophys Res 113:D13103. https://doi.org/10.1029/2008JD009944

Instituto Nacional De Pesquisas Espaciais (2014) (2014) Monitoramento da Floresta Amazônica Brasileira por Satélite: 2014

Jones DA, Simmonds I (1993) A climatology of Southern Hemisphere extratropical cyclones. Clim Dyn 9:131–145. https://doi.org/10.1007/BF00209750

Juárez RIN, Hodnett MG, Fu R et al (2007) Control of dry season evapotranspiration over the amazonian forest as inferred from observations at a Southern Amazon forest site. J Clim 20:2827–2839. https://doi.org/10.1175/JCLI4184.1

Junquas C, Heredia MB, Condom T et al (2022) Regional climate modeling of the diurnal cycle of precipitation and associated atmospheric circulation patterns over an Andean glacier region (Antisana, Ecuador). Clim Dyn. https://doi.org/10.1007/s00382-021-06079-y

Kendon EJ, Roberts NM, Senior CA, Roberts MJ (2012) Realism of rainfall in a very high-resolution regional climate model. J Clim 25:5791–5806. https://doi.org/10.1175/JCLI-D-11-00562.1

Khand K, Numata I, Kjaersgaard J, Vourlitis G (2017) Dry season evapotranspiration dynamics over human-impacted landscapes in the southern amazon using the landsat-based METRIC model. Remote Sens 9:706. https://doi.org/10.3390/rs9070706

Krinner G, Viovy N, de Noblet-Ducoudré N et al (2005) A dynamic global vegetation model for studies of the coupled atmosphere-biosphere system. Global Biogeochem Cycles. https://doi.org/10.1029/2003GB002199

Laipelt L, Ruhoff AL, Fleischmann AS et al (2020) Assessment of an automated calibration of the SEBAL algorithm to estimate dry-season surface-energy partitioning in a forest-savanna transition in Brazil. Remote Sens 12:1108. https://doi.org/10.3390/rs12071108

Lamarche C, Santoro M, Bontemps S et al (2017) Compilation and validation of SAR and optical data products for a complete and global map of inland/ocean water tailored to the climate modeling community. Remote Sens 9:36. https://doi.org/10.3390/rs9010036

Latrubesse EM, Arima EY, Dunne T et al (2017) Damming the rivers of the Amazon basin. Nature 546:363–369. https://doi.org/10.1038/nature22333

Lean J, Rowntree PR (1997) Understanding the sensitivity of a GCM simulation of amazonian deforestation to the specification of vegetation and soil characteristics. J Clim 10:1216–1235. https://doi.org/10.1175/1520-0442(1997)010%3c1216:UTSOAG%3e2.0.CO;2

Lee J-E, Lintner BR, Boyce CK, Lawrence PJ (2011) Land use change exacerbates tropical South American drought by sea surface temperature variability. Geophys Res Lett. https://doi.org/10.1029/2011GL049066

Leite CC, Costa MH, de Lima CA et al (2011) Historical reconstruction of land use in the Brazilian Amazon (1940–1995). J Land Use Sci 6:33–52. https://doi.org/10.1080/1747423X.2010.501157

Li W, Fu R, Dickinson RE (2006) Rainfall and its seasonality over the Amazon in the 21st century as assessed by the coupled models for the IPCC AR4. J Geophys Res: Atmos 111(D2). https://doi.org/10.1029/2005JD006355

Li W, Fu R (2004) Transition of the large-scale atmospheric and land surface conditions from the dry to the wet season over Amazonia as diagnosed by the ECMWF re-analysis. J Clim

17:2637–2651. https://doi.org/10.1175/1520-0442(2004)017%3c2637:TOTLAA%3e2.0.CO;2
Li W, Fu R (2006) Influence of cold air intrusions on the wet season onset over Amazonia. J Clim 19:257–275. https://doi.org/10.1175/JCLI3614.1
Liebmann B, Marengo J (2001) Interannual variability of the rainy season and rainfall in the Brazilian Amazon basin. J Clim 14:4308–4318. https://doi.org/10.1175/1520-0442(2001)014%3c4308:IVOTRS%3e2.0.CO;2
Lohou F, Kergoat L, Guichard F et al (2014) Surface response to rain events throughout the West African monsoon. Atmos Chem Phys 14:3883–3898. https://doi.org/10.5194/acp-14-3883-2014
Machado LAT, Laurent H, Dessay N, Miranda I (2004) Seasonal and diurnal variability of convection over the Amazonia: a comparison of different vegetation types and large scale forcing. Theor Appl Climatol. https://doi.org/10.1007/s00704-004-0044-9
Maeda EE, Ma X, Wagner FH et al (2017) Evapotranspiration seasonality across the Amazon Basin. Earth Syst Dyn 8:439–454. https://doi.org/10.5194/esd-8-439-2017
Maignan F, Bréon F-M, Chevallier F et al (2011) Evaluation of a global vegetation model using time series of satellite vegetation indices. Geosci Model Dev 4:1103–1114. https://doi.org/10.5194/gmd-4-1103-2011
Malhi Y, Wright J (2004) Spatial patterns and recent trends in the climate of tropical rainforest regions. Philos Trans R Soc London Ser B Biol Sci 359:311–329. https://doi.org/10.1098/rstb.2003.1433
Malhi Y, Roberts JT, Betts RA et al (2008) Climate change, deforestation, and the fate of the Amazon. Science (80-) 319:169–172. https://doi.org/10.1126/science.1146961
Marengo JA, Espinoza JC (2016) Extreme seasonal droughts and floods in Amazonia: causes, trends and impacts. Int J Climatol 36:1033–1050. https://doi.org/10.1002/joc.4420
Marengo JA, Liebmann B, Kousky VE et al (2001) Onset and end of the rainy season in the Brazilian Amazon basin. J Clim 14:833–852. https://doi.org/10.1175/1520-0442(2001)014%3c0833:OAEOTR%3e2.0.CO;2
Marengo JA, Fisch GF, Alves LM et al (2017) Meteorological context of the onset and end of the rainy season in Central Amazonia during the GoAmazon2014/5. Atmos Chem Phys 17:7671–7681. https://doi.org/10.5194/acp-17-7671-2017
Melack JM, Basso LS, Fleischmann AS et al (2022) Challenges regionalizing methane emissions using aquatic environments in the Amazon basin as examples. Front Environ Sci. https://doi.org/10.3389/fenvs.2022.866082
Michelangeli P-A, Vautard R, Legras B (1995) Weather regimes: recurrence and quasi stationarity. J Atmos Sci 52:1237–1256. https://doi.org/10.1175/1520-0469(1995)052%3c1237:WRRAQS%3e2.0.CO;2
Miguez-Macho G, Stenchikov GL, Robock A (2004) Spectral nudging to eliminate the effects of domain position and geometry in regional climate model simulations. J Geophys Res Atmos. https://doi.org/10.1029/2003JD004495
Molina-Carpio J, Espinoza JC, Vauchel P et al (2017) Hydroclimatology of the Upper Madeira River basin: spatio-temporal variability and trends. Hydrol Sci J 62:911–927. https://doi.org/10.1080/02626667.2016.1267861
Moron V, Robertson AW, Ward MN, Ndiaye O (2008) Weather types and rainfall over Senegal. Part I: observational analysis. J Clim 21:266–287. https://doi.org/10.1175/2007JCLI1601.1
Moron V, Robertson AW, Qian J-H, Ghil M (2015) Weather types across the Maritime Continent: from the diurnal cycle to interannual variations. Front Environ Sci. https://doi.org/10.3389/fenvs.2014.00065
Morrison H, Thompson G, Tatarskii V (2009) Impact of cloud microphysics on the development of trailing stratiform precipitation in a simulated squall line: comparison of one- and two-moment schemes. Mon Weather Rev 137:991–1007. https://doi.org/10.1175/2008MWR2556.1
Muñoz-Sabater J, Dutra E, Agustí-Panareda A et al (2021) ERA5-Land: a state-of-the-art global reanalysis dataset for land applications. Earth Syst Sci Data 13:4349–4383. https://doi.org/10.5194/essd-13-4349-2021
Myneni RB, Yang W, Nemani RR et al (2007) Large seasonal swings in leaf area of Amazon rainforests. Proc Natl Acad Sci 104:4820–4823. https://doi.org/10.1073/pnas.0611338104
Nakanishi M, Niino H (2006) An improved mellor-yamada level-3 model: its numerical stability and application to a regional prediction of advection fog. Boundary-Layer Meteorol 119:397–407. https://doi.org/10.1007/s10546-005-9030-8
Negri AJ, Adler RF, Xu L, Surratt J (2004) The impact of Amazonian deforestation on dry season rainfall. J Clim 17:1306–1319. https://doi.org/10.1175/1520-0442(2004)017%3c1306:TIOADO%3e2.0.CO;2
Neill C, Coe MT, Riskin SH et al (2013) Watershed responses to Amazon soya bean cropland expansion and intensification. Philos Trans R Soc B Biol Sci 368:20120425. https://doi.org/10.1098/rstb.2012.0425
Nepstad DC, Stickler CM, Soares-Filho B, Merry F (2008) Interactions among Amazon land use, forests and climate: prospects for a near-term forest tipping point. Philos Trans R Soc B Biol Sci 363:1737–1746. https://doi.org/10.1098/rstb.2007.0036
Nobre CA, Sellers PJ, Shukla J (1991) Amazonian deforestation and regional climate change. J Clim. https://doi.org/10.1175/1520-0442(1991)004%3c0957:adarcc%3e2.0.co;2
Nobre CA, Sampaio G, Borma LS et al (2016) Land-use and climate change risks in the amazon and the need of a novel sustainable development paradigm. Proc Natl Acad Sci USA 113:10759–10768. https://doi.org/10.1073/pnas.1605516113
Oliveira G, Brunsell NA, Moraes EC et al (2019) Effects of land-cover changes on the partitioning of surface energy and water fluxes in Amazonia using high-resolution satellite imagery. Ecohydrology. https://doi.org/10.1002/eco.2126
Olmo ME, Espinoza J-C, Bettolli ML et al (2022) Circulation patterns and associated rainfall over south tropical south America: GCMs evaluation during the dry-to-wet transition season. J Geophys Res Atmos. https://doi.org/10.1029/2022JD036468
Omrani H, Drobinski P, Dubos T (2015) Using nudging to improve global-regional dynamic consistency in limited-area climate modeling: what should we nudge? Clim Dyn 44:1627–1644. https://doi.org/10.1007/s00382-014-2453-5
Ortega G, Arias PA, Villegas JC et al (2021) Present-day and future climate over central and South America according to CMIP5/CMIP6 models. Int J Climatol 41:6713–6735. https://doi.org/10.1002/joc.7221
Paccini L, Espinoza JC, Ronchail J, Segura H (2018) Intra-seasonal rainfall variability in the Amazon basin related to large-scale circulation patterns: a focus on western Amazon-Andes transition region. Int J Climatol 38:2386–2399. https://doi.org/10.1002/joc.5341
Pedregosa F, Varoquaux G, Gramfort A et al (2011) Scikit-learn: machine learning in python. J Mach Learn Res 12:2825–2830
Perugini L, Caporaso L, Marconi S et al (2017) Biophysical effects on temperature and precipitation due to land cover change. Environ Res Lett. https://doi.org/10.1088/1748-9326/aa6b3f
Phillips OL, Aragão LEOC, Lewis SL et al (2009) Drought sensitivity of the Amazon rainforest. Science (80-) 323:1344–1347. https://doi.org/10.1126/science.1164033
Pichelli E, Coppola E, Sobolowski S et al (2021) The first multimodel ensemble of regional climate simulations at kilometer-scale resolution part 2: historical and future simulations of

precipitation. Clim Dyn 56:3581–3602. https://doi.org/10.1007/s00382-021-05657-4
Pires GF, Abrahão GM, Brumatti LM, Oliveira LJ, Costa MH, Liddicoat S et al (2016) Increased climate risk in Brazilian double cropping agriculture systems: implications for land use in Northern Brazil. Agric For Meteorol 228:286–298. https://doi.org/10.1016/j.agrformet.2016.07.005
Polcher J (1995) Sensitivity of tropical convection to land surface processes. J Atmos Sci 52:3143–3161. https://doi.org/10.1175/1520-0469(1995)052%3c3143:SOTCTL%3e2.0.CO;2
Polcher J, Laval K (1994) The impact of African and Amazonian deforestation on tropical climate. J Hydrol 155:389–405. https://doi.org/10.1016/0022-1694(94)90179-1
Posada-Marín JA, Rendón AM, Salazar JF et al (2019) WRF downscaling improves ERA-Interim representation of precipitation around a tropical Andean valley during El Niño: implications for GCM-scale simulation of precipitation over complex terrain. Clim Dyn 52:3609–3629. https://doi.org/10.1007/s00382-018-4403-0
Rochedo PR, Soares-Filho B, Schaeffer R, Viola E, Szklo A, Lucena AF et al (2018) The threat of political bargaining to climate mitigation in Brazil. Nat Clim Change 8(8):695–698. https://doi.org/10.1038/s41558-018-0213-y
Rosales AG, Junquas C, da Rocha RP et al (2022) Valley-mountain circulation associated with the diurnal cycle of precipitation in the tropical Andes (Santa River Basin, Peru). Atmosphere (basel) 13:344. https://doi.org/10.3390/atmos13020344
Ruiz-Vásquez M, Arias PA, Martínez JA, Espinoza JC (2020) Effects of Amazon basin deforestation on regional atmospheric circulation and water vapor transport towards tropical South America. Clim Dyn 54:4169–4189. https://doi.org/10.1007/s00382-020-05223-4
Saavedra M, Junquas C, Espinoza JC, Silva Y (2020) Impacts of topography and land use changes on the air surface temperature and precipitation over the central Peruvian Andes. Atmos Res 234:104711. https://doi.org/10.1016/j.atmosres.2019.104711
Salati E, Dall'Olio A, Matsui E, Gat JR (1979) Recycling of water in the Amazon Basin: an isotopic study. Water Resour Res 15:1250–1258. https://doi.org/10.1029/WR015i005p01250
Salazar LF, Nobre CA, Oyama MD (2007) Climate change consequences on the biome distribution in tropical South America. Geophys Res Lett. https://doi.org/10.1029/2007GL029695
Saleska SR, da Rocha HR, Huete AR et al (2013) LBA-ECO CD-32 flux tower network data compilation. Brazilian Amazon. https://doi.org/10.3334/ORNLDAAC/1174
Schrapffer A (2022) High-resolution numerical analysis of land-river-floodplains-atmosphere interaction in La Plata Basin. Universidad de Buenos Aires, Institut Polytechnique de Paris
Shukla J, Nobre C, Sellers P (1990) Amazon deforestation and climate change. Science (80-). https://doi.org/10.1126/science.247.4948.1322
Shukla PR, Skeg J, Buendia EC, et al (2019) Climate Change and Land: an IPCC special report on climate change, desertification, land degradation, sustainable land management, food security, and greenhouse gas fluxes in terrestrial ecosystems.
Sierra JP, Arias PA, Vieira SC (2015) Precipitation over Northern South America and its seasonal variability as simulated by the CMIP5 models. Adv Meteorol 2015:1–22. https://doi.org/10.1155/2015/634720
Sierra JP, Junquas C, Espinoza JC et al (2021) Deforestation impacts on Amazon-Andes hydroclimatic connectivity. Clim Dyn. https://doi.org/10.1007/s00382-021-06025-y
Silva Dias MAF, Regnie P (1996) Simulation of mesoscale circulations in a deforested area of Rondonia in the dry season. In: Gash JHC (ed) Amazonian Deforestation and Climate. Oxford University Press, pp 531–547
Sinclair MR (1995) A climatology of cyclogenesis for the southern hemisphere. Mon Weather Rev 123:1601–1619. https://doi.org/10.1175/1520-0493(1995)123%3c1601:ACOCFT%3e2.0.CO;2
Siqueira JR, Toledo Machado LA (2004) Influence of the frontal systems on the day-to-day convection variability over South America. J Clim 17:1754–1766. https://doi.org/10.1175/1520-0442(2004)017%3c1754:IOTFSO%3e2.0.CO;2
Skamarock WC, Klemp JB, Dudhia J, Gill DO, Barker DM, Duda MG, Huang XY, Wang W, Powers JG (2008) A description of the advanced research WRF Version 3. Note NCAR/TN-475+ STR, NCAR Tech, Colorado. https://doi.org/10.5065/D68S4MVH
Smith CB, Lakhtakia MN, Capehart WJ, Carlson TN (1994) Initialization of soil-water content in regional-scale atmospheric prediction models. Bull Am Meteorol Soc 75:585–593. https://doi.org/10.1175/1520-0477(1994)075%3c0585:IOSWCI%3e2.0.CO;2
Soares-Filho BS, Nepstad DC, Curran LM et al (2006) Modelling conservation in the Amazon basin. Nature 440:520–523. https://doi.org/10.1038/nature04389
Sombroek W (2001) Spatial and temporal patterns of Amazon rainfall. AMBIO A J Hum Environ 30:388–396. https://doi.org/10.1579/0044-7447-30.7.388
Sommer R, Sá, Vielhauer K TD et al (2002) Transpiration and canopy conductance of secondary vegetation in the eastern Amazon. Agric for Meteorol 112:103–121. https://doi.org/10.1016/S0168-1923(02)00044-8
Sörensson AA, Ruscica RC (2018) Intercomparison and uncertainty assessment of nine evapotranspiration estimates over South America. Water Resour Res 54:2891–2908. https://doi.org/10.1002/2017WR021682
Souza EP, Renno NO, Dias MAFS (2000) Convective circulations induced by surface heterogeneities. J Atmos Sci 57:2915–2922. https://doi.org/10.1175/1520-0469(2000)057%3c2915:CCIBSH%3e2.0.CO;2
Souza CM, Shimbo JZ, Rosa MR, Parente LL, Alencar AA, Rudorff BFT et al (2020) Reconstructing three decades of land use and land cover changes in brazilian biomes with landsat archive and earth engine. Remote Sens 12(17):2735. https://doi.org/10.3390/rs12172735
Spera SA, Winter JM, Chipman JW (2018) Evaluation of agricultural land cover representations on regional climate model simulations in the Brazilian Cerrado. J Geophys Res Atmos 123:5163–5176. https://doi.org/10.1029/2017JD027989
Staal A, Tuinenburg OA, Bosmans JHC et al (2018) Forest-rainfall cascades buffer against drought across the Amazon. Nat Clim Chang 8:539–543. https://doi.org/10.1038/s41558-018-0177-y
Staver AC, Archibald S, Levin SA (2011) The global extent and determinants of savanna and forest as alternative biome states. Science (80-) 334:230–232. https://doi.org/10.1126/science.1210465
Sud YC, Lau WK-M, Walker GK et al (1996) Biogeophysical consequences of a tropical deforestation scenario: a GCM simulation study. J Clim 9:3225–3247. https://doi.org/10.1175/1520-0442(1996)009%3c3225:BCOATD%3e2.0.CO;2
Sutton C, Hamill TM, Warner TT (2006) Will perturbing soil moisture improve warm-season ensemble forecasts? A proof of concept. Mon Weather Rev 134:3174–3189. https://doi.org/10.1175/MWR3248.1
Swann ALS, Longo M, Knox RG et al (2015) Future deforestation in the Amazon and consequences for South American climate. Agric for Meteorol 214–215:12–24. https://doi.org/10.1016/j.agrformet.2015.07.006
Taylor KE (2001) Summarizing multiple aspects of model performance in a single diagram. J Geophys Res Atmos 106:7183–7192. https://doi.org/10.1029/2000JD900719
Taylor CM, Ellis RJ (2006) Satellite detection of soil moisture impacts on convection at the mesoscale. Geophys Res Lett 33:L03404. https://doi.org/10.1029/2005GL025252

Trachte K (2018) Atmospheric moisture pathways to the highlands of the tropical andes: analyzing the effects of spectral nudging on different driving fields for regional climate modeling. Atmosphere (Basel) 9:456. https://doi.org/10.3390/atmos9110456

Van Der Ent RJ, Savenije HHG, Schaefli B, Steele-Dunne SC (2010) Origin and fate of atmospheric moisture over continents. Water Resour Res. https://doi.org/10.1029/2010WR009127

Voldoire A, Sanchez-Gomez E, Salas y Mélia D, et al (2013) The CNRM-CM5.1 global climate model: description and basic evaluation. Clim Dyn 40:2091–2121. https://doi.org/10.1007/s00382-011-1259-y

von Randow C, Manzi AO, Kruijt B et al (2004) Comparative measurements and seasonal variations in energy and carbon exchange over forest and pasture in South West Amazonia. Theor Appl Climatol 78:5–26. https://doi.org/10.1007/s00704-004-0041-z

von Randow RCS, Tomasella J, von Randow C et al (2020) Evapotranspiration and gross primary productivity of secondary vegetation in Amazonia inferred by eddy covariance. Agric For Meteorol 294:108141. https://doi.org/10.1016/j.agrformet.2020.108141

von Storch H, Langenberg H, Feser F (2000) A spectral nudging technique for dynamical downscaling purposes. Mon Weather Rev 128:3664–3673. https://doi.org/10.1175/1520-0493(2000)128%3c3664:ASNTFD%3e2.0.CO;2

Wang H, Fu R (2002) Cross-equatorial flow and seasonal cycle of precipitation over South America. J Clim 15:1591–1608. https://doi.org/10.1175/1520-0442(2002)015%3c1591:CEFASC%3e2.0.CO;2

Wang J, Chagnon FJF, Williams ER et al (2009) Impact of deforestation in the Amazon basin on cloud climatology. Proc Natl Acad Sci USA 106:3670–3674. https://doi.org/10.1073/pnas.0810156106

Wang C, Qian Y, Duan Q et al (2021) Quantifying physical parameterization uncertainties associated with land-atmosphere interactions in the WRF model over Amazon. Atmos Res 262:105761. https://doi.org/10.1016/j.atmosres.2021.105761

Wongchuig Correa S, de Paiva RCD, Espinoza JC, Collischonn W (2017) Multi-decadal hydrological retrospective: case study of amazon floods and droughts. J Hydrol 549:667–684. https://doi.org/10.1016/j.jhydrol.2017.04.019

Wright IR, Gash JHC, Da Rocha HR et al (1992) Dry season micrometeorology of central Amazonian Ranchland. Q J R Meteorol Soc 118:1083–1099. https://doi.org/10.1002/qj.49711850804

Wright JS, Fu R, Worden JR et al (2017) Rainforest-initiated wet season onset over the southern Amazon. Proc Natl Acad Sci 114:8481–8486. https://doi.org/10.1073/pnas.1621516114

Yin L, Fu R, Zhang Y-F et al (2014) What controls the interannual variation of the wet season onsets over the Amazon? J Geophys Res Atmos 119:2314–2328. https://doi.org/10.1002/2013JD021349

Yoon JH, Zeng N (2010) An Atlantic influence on Amazon rainfall. Clim Dyn. https://doi.org/10.1007/s00382-009-0551-6

Zemp DC, Schleussner CF, Barbosa HMJ et al (2014) On the importance of cascading moisture recycling in South America. Atmos Chem Phys. https://doi.org/10.5194/acp-14-13337-2014

Zeng N, Neelin JD (1999) A land-atmosphere interaction theory for the tropical deforestation problem. J Clim 12:857–872. https://doi.org/10.1175/1520-0442(1999)012%3c0857:ALAITF%3e2.0.CO;2

Zhang S, Zhang K, Wan H, Sun J (2022) Further improvement and evaluation of nudging in the E3SM Atmosphere Model version 1 (EAMv1). Geosci Model Dev Discuss. https://doi.org/10.5194/gmd-2022-10

Zhang H, McGuffie K, Henderson-Sellers A (1996) Impacts of tropical deforestation. Part II: the role of large-scale dynamics. J Clim. https://doi.org/10.1175/1520-0442(1996)009<2498:IOTDPI>2.0.CO;2